Palaeogeography, Palaeoclimatology, Palaeoecology 623 (2023) 111632

Contents lists available at ScienceDirect

Palaeogeography, Palaeoclimatology, Palaeoecology

journal homepage: www.elsevier.com/locate/palaeo

Late Eocene to late Oligocene terrestrial climate and vegetation change in the western Tasmanian region

Michael Amoo [a,*], Ulrich Salzmann [a], Matthew J. Pound [a], Frida S. Hoem [b], Nick Thompson [a], Peter K. Bijl [b]

[a] Department of Geography and Environmental Sciences, Northumbria University, Newcastle upon Tyne, UK
[b] Department of Earth Science, Utrecht University, Utrecht, the Netherlands

ARTICLE INFO

Editor: Dr. Howard Falcon-Lang

Keywords:
Eocene-Oligocene transition
Pollen
Climate estimate
Tectonic
Tasmanian Gateway
CO_2

ABSTRACT

While many palaeoclimate studies have focussed on the Eocene-Oligocene transition (EOT), little is known about the timing and drivers of the post-EOT climate recovery. To better understand and reconstruct terrestrial climate and vegetation dynamics from the late Eocene to late Oligocene (35.5–27.46 Ma), we use a new, high-resolution palynological record and quantitative sporomorph-based climate estimates recovered from ODP Site 1168 on the western Tasmanian margin. Late Eocene (35.50–34.81 Ma) floras reveal *Nothofagus*-dominated temperate forests with secondary *Gymnostoma* and minor thermophilic plant elements growing under wet conditions, with mean annual temperatures (MATs) of ~13 °C. This is followed by a small decrease in terrestrial temperatures across the EOT by ~2 °C. Apart from a slight decline in abundance of *Gymnostoma*, increases in the *Fuscospora* and *Lophozonia*-type *Nothofagus,* and the disappearance of palms (Arecaceae), vegetation remained relatively stable across the EOT. However, a prolonged interval of warm-temperate conditions after 33.0 Ma, independent of fluctuations in the current pCO_2 record, imply additional regional controls on local climate. Changes in surface oceanographic currents, due to sustained deepening of the Tasmanian Gateway, may have played a significant role in sustaining warm-temperate vegetation in southern Australia post-EOT. The early Oligocene (PZ 3; 30.5–27.46 Ma) vegetation record still maintains the *Nothofagus*-dominated forest with a recovery in *Gymnostoma*. Gymnosperms (especially Araucariaceae, *Dacrydium*, and *Podocarpus*) and cryptogams expanded alongside an increase in overall species diversity. Sporomorph-based MATs averaged ~11 °C in this interval. The expansion of cool-temperate forest (sustained cool-temperate climate conditions in our terrestrial records) matches the general declining pCO_2 concentrations in the early Oligocene. The synchroneity between terrestrial and marine temperatures (MATs and SSTs gradually decline) and atmospheric pCO_2 highlight the importance of pCO_2 in driving terrestrial climate and vegetation change in the Tasmanian region during the early Oligocene.

1. Introduction

Earth's climate is reported to have undergone major changes during the late Eocene to early Oligocene that ultimately led to a transition from a greenhouse to an icehouse world (Pearson et al., 2009; Villa et al., 2014; Galeotti et al., 2016; Hutchinson et al., 2021). The long-term late Eocene cooling trend peaked at the Eocene-Oligocene Transition (EOT; 34.44–33.65 Ma; Katz et al., 2008; Pound and Salzmann, 2017; Hutchinson et al., 2021), marked by the positive excursion in $\delta^{18}O$ of benthic foraminifera (Zachos et al., 2001; Westerhold et al., 2020). Two main mechanisms have been proposed as possible drivers for this transition from a greenhouse to an icehouse world (Lauretano et al., 2021). Whereas earlier studies attributed the EOT cooling to the opening of Southern Ocean gateways (Tasmanian gateway and Drake Passage; Kennett, 1977), later studies have ascribed this cooling to declining pCO_2 (Deconto and Pollard, 2003; Anagnostou et al., 2016; Cramwinckel et al., 2018; Lauretano et al., 2021). Aside from these mechanisms proposed as potential climate drivers, others such as deep-water formation and CO_2 sequestration due to a strengthening of Atlantic Meridional Overturning Circulation (Elsworth et al., 2017; Hutchinson et al., 2021) are thought to have provided the necessary pre-conditions for global cooling.

A late Eocene - early Oligocene marine pollen and spore record from ODP Site 1172 on the East Tasman Plateau (ETP) suggests that surface

* Corresponding author.
E-mail address: michael.amoo@northumbria.ac.uk (M. Amoo).

https://doi.org/10.1016/j.palaeo.2023.111632
Received 29 July 2022; Received in revised form 6 May 2023; Accepted 6 May 2023
Available online 9 May 2023

oceanographic changes most likely had knock-on effects. These changes were due to the accelerated deepening of the Tasmanian Gateway and atmospheric pCO_2, which drove terrestrial climate and vegetation change in eastern Tasmania (Amoo et al., 2022a). Evidence of this is seen in the fluctuation between cool and warm-temperate climate conditions with MATs between 11 and 15 °C (35.5–34.59 Ma), cooling across the EOT, and climate recovery post-EOT (Amoo et al., 2022a). However, a gap in the palynomorph record of ODP Site 1172 between ca. 33 and 30 Ma due to a series of sedimentary hiatuses and palynomorph barrenness, hampers a detailed reconstruction of vegetation and climate in Tasmania after the EOT (Amoo et al., 2022a). This limitation places a further constraint on identification of the potential driver(s) of the terrestrial post-EOT climate recovery. In addition, two published Eocene and Oligocene vegetation and climate reconstructions from southeastern Australia (Gippsland Basin) report contrasting Oligocene climates with one indicating uniform microthermic conditions throughout the Oligocene (Korasidis et al., 2019), whereas Sluiter et al. (2022) suggest predominantly mesothermic condition. Differences in dating as well as palaeoclimate estimation techniques between the two studies may be responsible for the disparate climate trends, especially in the Oligocene (Sluiter et al., 2022). Additional southern Australian (regional) vegetation and terrestrial climate records across the Eocene and particularly the Oligocene, are sparse and often poorly dated (Macphail et al., 1994; Macphail, 2007; Bijl et al., 2021; Lauretano et al., 2021).

Here, we present a new, well-dated, high-resolution pollen record and sporomorph-derived climate estimates recovered from marine ODP Site 1168 (Fig. 1a) on the western margin of Tasmania spanning the late Eocene (35.5 Ma) to early-late Oligocene (27.46 Ma) to reconstruct vegetation and climate. High-resolution model simulations, seismic, and geochemical data (Stickley et al., 2004; Sijp et al., 2011, 2014; Sauermilch et al., 2019; Sauermilch et al., 2021) suggest that the accelerated deepening and widening of the Tasmanian Gateway between ~35.50 and 30.20 Ma controlled and strengthened ocean current circulation, and throughflow of the proto-Leeuwin Current (PLC; Fig. 1b). By the early Oligocene, the disappearance of Antarctic-derived peridinioid cysts and increase in cosmopolitan dinoflagellate cyst (dinocyst) taxa on the eastern side of the Tasmania Gateway (ODP Site 1172) is reported to have been caused by the throughflow of the PLC (Sluijs et al., 2003). Site 1168 was under the influence of warm waters associated with the PLC throughout the Eocene and Oligocene (Exon et al., 2001; Stickley et al., 2004; Holdgate et al., 2017; Hoem et al., 2021), whereas ODP Site 1172 and Gippsland Basin sites were facing the cool Tasman Current (TC; cool surface currents associated with the proto-Ross Gyre) of the Pacific Ocean until ~35.5 Ma (latest Eocene; Stickley et al., 2004; Houben et al., 2019; Holdgate et al., 2017). Their palaeogeographic positions are reported to have resulted in different climate regimes separating the cooler and wetter eastern Tasmania (responding to the cooler proto-Ross Sea Gyre) and a warm-wet western Tasmania (Site 1168) linked to warm water currents associated with the PLC (Holdgate et al., 2017). The late Eocene to early Oligocene sporomorph records from the western Tasmanian margin (ODP Site 1168) are thus a key to further our understanding of the terrestrial climate and vegetation on Tasmania during this time interval.

By comparing our new sporomorph record with Site 1172 (Amoo et al., 2022a), we will test whether the sustained deepening and widening of the Tasmanian Gateway during the early Oligocene coincides with major reorganisation of climate and vegetation at Site 1168 (western Tasmania). We hypothesise that the latest Eocene-early Oligocene tectonic deepening and widening of the Tasmanian Gateway leading to the throughflow of the PLC into the southwest Pacific and equatorward movement of the Australian landmass must have influenced terrestrial climate and vegetation in western Tasmania (Site 1168).

2. Materials and methods

2.1. Tectonic evolution and study site

The Cretaceous to middle Eocene separation of Australia from Antarctica resulted in the formation of the Australo-Antarctic Gulf (AAG; Gaina et al., 1998; Shipboard Scientific Party, 2001) and the northwest movement of Tasmania. The resulting epicontinental basin formed between Antarctica and Tasmania is divided into a series of narrow basins by the northwest-southeast strike-slip faulting in western Tasmania. This further led to the formation of a margin around western Tasmania (WT; Shipboard Scientific Party, 2001). Our study site (ODP Site 1168) is one of the five sites drilled during the Ocean Drilling

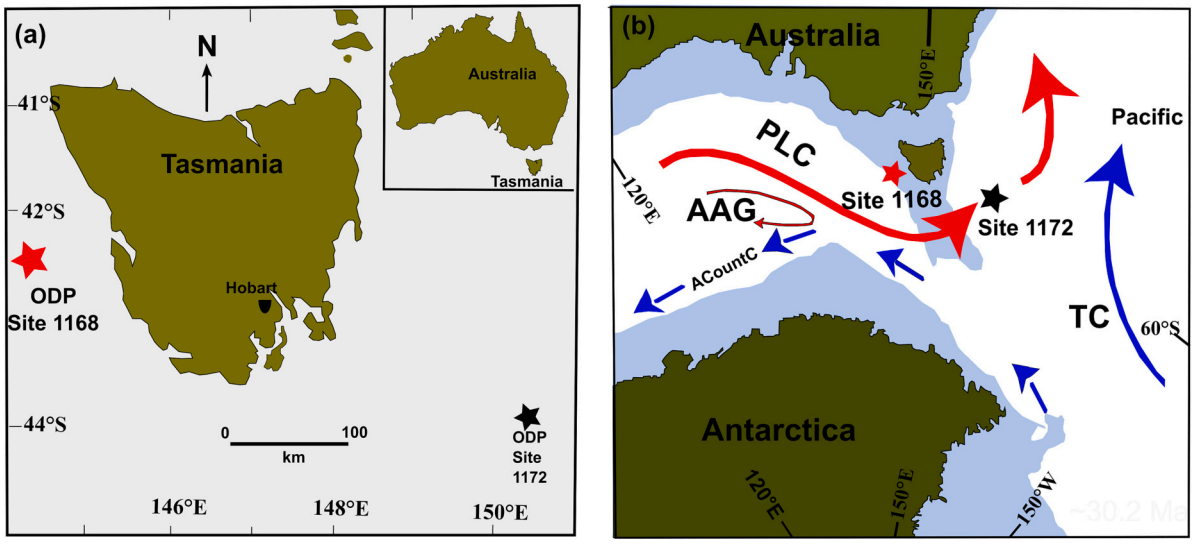

Fig. 1. (a) Present-day Tasmania and locations of the western margin of Tasmania (ODP Site 1168; red star) and East Tasman Plateau (ODP Site 1172; black star) after Quilty (2001). ODP Site 1168 is submerged at a water depth of ~2463 m and ODP Site 1172 at a water depth of ~2620 m. ODP Site 1168 is the subject of this study and Site 1172 was the subject of Amoo et al. (2022a). (b) Tasmanian Gateway palaeoceanography and palaeogeography during the early Oligocene. Surface ocean currents are modified after reconstructions by Stickley et al. (2004). TC: Tasman current, PLC: proto-Leeuwin current, ACountC: Antarctic Counter Current, AAG: Australo-Antarctic Gulf. Red arrows indicate warmer surface currents associated with the PLC, and blue arrows show cooler surface currents associated with the proto-Ross Gyre. (For interpretation of the references to colour in this figure legend, the reader is referred to the web version of this article.)

Program (ODP) Leg 189 expedition around Tasmania (Shipboard Scientific Party, 2001). The goal of the expedition was to investigate and provide, with accuracy, the timing and climatic implications of the opening of the Tasmanian Gateway (Shipboard Scientific Party, 2001). This opening resulted in the deepwater connection between the Indian and southwest Pacific oceans and the development of the Tasman Seaway (Fig. 1a; Exon et al., 2001). Site 1168 is located in the Sorell Basin, ~70 km offshore on the western margin of Tasmania (42°38′S, 144°25′ E; Fig. 1a) at a water depth of 2463 m (Exon et al., 2001). However, during the late Eocene and early Oligocene, the western margin of Tasmania was located between 63 and 57°S (van Hinsbergen et al., 2015; Cande and Stock, 2004). In contrast to other ODP sites sampled during Leg 189, spores and pollen are more abundant than dinoflagellate cysts, suggesting a higher runoff and closer proximity of Site 1168 to a river outlet (Exon et al., 2004; Hill and Exon, 2004).

Lithologically, the marine sedimentary unit is divided into: (1) organic-rich, shallow-marine brown and grey mid-Eocene to late Eocene silty mudstones (Unit V; until 788.76 m below sea floor (b.s.f.)); (2) a condensed late Eocene to earliest Oligocene transitional unit with high glauconite (greensand) content (upper unit IV to III; 749.4–666.6 m b.s.f.); and (3) a calcareous succession mainly composed of nannofossil ooze deposited during the Oligocene (Unit II; 340–660 m b.s.f.; Exon et al., 2001). A detailed description of the depositional and oceanographic setting is given in Hoem et al. (2021). ODP Hole 1168A on the western margin of Tasmania yielded EOT records that have been analysed for their sporomorph content in this study. The age model relies on palaeomagnetic and biostratigraphic events in the dinocyst, foraminifera and calcareous nannofossil records (Pfuhl and McCave, 2003; Sluijs et al., 2003; Stickley et al., 2004; Pross et al., 2012; Houben et al., 2019; Hoem et al., 2021).

2.2. Sample preparation and pollen analysis

A total of 51 samples from the late Eocene to early late Oligocene of ODP Site 1168 (35.50–27.46 Ma) were studied for their sporomorph content to reconstruct past vegetation and climate. The processing of samples for palynological analyses followed the standard procedures at the GeoLab, Utrecht University (Brinkhuis et al., 2003; Bijl et al., 2018). Sample processing involved crushing and weighing (on average 10 g) of dried samples before treating with 30% cold hydrochloric acid and 38% hydrofluoric acid to remove carbonate and silicate minerals, respectively. The remaining palynological residue was then sieved through a 10 and 15 μm nylon mesh to remove unwanted organic/inorganic matter. The residues were then transferred onto microscope slides with glycerine gel as the mounting medium and sealed with nail polish.

Leica DM 500 and DM 2000 LED transmitted light microscopes were used to count two slides for each sample under 400× and 1000× magnification. Where possible, 250 fossil spores and pollen specimens (excluding reworking) were counted for each sample. The whole microscope slide was then scanned for rare taxa. Twelve out of 51 samples were excluded from further analysis due to lack of sporomorph grains (<75 specimens). Reworked sporomorphs were identified based on the colour of their exine and occurrence beyond their known stratigraphic range (Contreras et al., 2014). Reworked sporomorphs were recorded, but not added to the total pollen and spore count (see Supplementary Information; Amoo et al., 2022b). Pollen percentages were calculated using the sum of total sporomorphs and plotted using Tilia version 2.6.1 (Fig. 2; Grimm, 1990). Sporomorph identification, taxonomic classification, and botanical affinities were carried out following Macphail and Cantrill (2006); Macphail (2007); Raine et al. (2011); Bowman et al. (2014); and Macphail and Hill (2018).

PAST statistical software (Hammer et al., 2001) was used to generate diversity indices (rarefaction, Shannon diversity, and equitability). Rarefaction was applied to remove the effect of differences in sampling size and allow the estimation of sporomorph species at a constant sample size (Birks and Line, 1992; Birks et al., 2016). The Shannon Diversity index (H) considers number of individuals as well as number of taxa, and evenness of the species present (Shannon, 1948). H varies from 0 involving vegetation communities with a single taxon to higher values where taxa are evenly distributed (Legendre and Legendre, 2012). Equitability (J) measures the level of abundance and how taxa are distributed in an assemblage. Low J values indicate the dominance of a few species in the population (Hayek and Buzas, 2010). Pollen Zones (PZ) have been defined following stratigraphically constrained cluster analysis (CONISS; Grimm, 1987), in Tilia (version. 2.6.1; Fig. 2) using total sum of squares with chord distance square root transformation (Cavalli-Sforza and Edwards, 1967; Grimm, 1987).

2.3. Multivariate statistical ordination techniques

The sporomorph percentage data (originally down weighted by removing pollen taxa <5%) were normalised and analysed using Detrended Correspondence Analysis (DCA) and Principal Component Analysis (PCA). These multivariate ordination techniques were used to assess how species and sample composition change and overlap through time across the studied section. DCA is a metric ordination tool that uses reciprocal averaging and allows the determination of species distribution in a two-dimensional space (Gauch, 1982). Species turnover across a sampling gradient (first axis length) that is greater than two standard deviation (> 2-SD) units, gives an indication of samples not having similar species (Gauch, 1982). However, where the first axis length of DCA is lower than 2-SD, it most likely suggests that species show linear distribution rather than unimodal (ter Braak and Šmilauer, 2002). As a result, the ordination techniques based on a linear response model such as PCA (Goodall, 1954) are suitable for "homogeneous" data sets. Both PCA and DCA were performed using the software R for statistical computing (R Core Team, 2019) and the vegan package (Oksanen et al., 2019).

2.4. Pollen-based climate reconstruction

Quantitative sporomorph-based climate estimates for mean annual temperature (MAT), warm mean month temperature (WMMT), cold month mean temperature (CMMT), and mean annual precipitation (MAP) were obtained using the nearest living relative (NLR) approach and the probability density function (PDF) method. The NLR, based on the principle of uniformitarianism, assumes that climate tolerance of living taxa can be extended into the past. The sporomorph-based climate estimates using the NLR relies on the presence or absence of pollen taxa hence independent of relative abundance of individual taxa. This serves as one of the main strengths of this method because it is particularly useful for deriving sporomorph-based climate estimates from marine sediments, where processes like hydrodynamic sorting of grains may lead to overrepresentation or underrepresentation of individual taxa (Thompson et al., 2022), while helping to reduce taphonomic biases (Klages et al., 2020).

The PDF method works by statistically constraining the most likely climate co-occurrence envelope for an assemblage (Harbert and Nixon, 2015; Klages et al., 2020). Bioclimatic envelopes were first identified for each NLR by cross-plotting their modern distribution from the Global Biodiversity Information Facility (GBIF, 2022) with gridding from WorldCLIM climate surface (Fick and Hijmans, 2017) using the dismo package in R (Hijmans et al., 2017). The datasets were then filtered to remove multiple entries per climate grid cell, plants whose botanical affinity are vague or doubtful, redundant, and occurrences termed exotic (e.g., garden plants). Filtering further removes bias in the probability function which may likely lead to results leaning towards a particular location (Reichgelt et al., 2018). To test the robustness of the dataset, bootstrapping was applied which was followed by calculating the likelihood of a taxon that occurs at a specific climate variable using the mean and standard deviation of modern range of each taxon (Kühl et al., 2002; Willard et al., 2019). In this study, climatic ranges are indicated

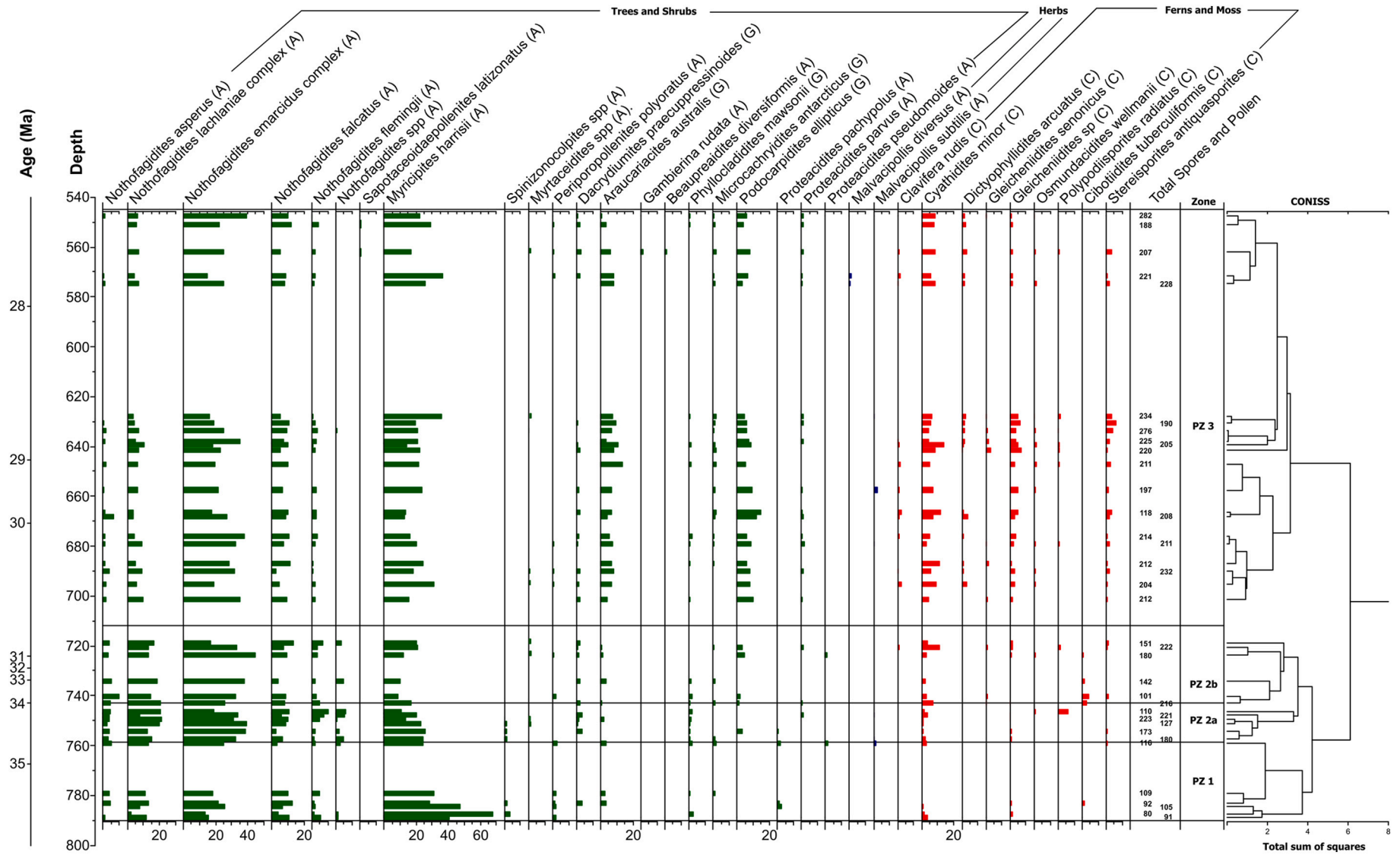

Fig. 2. Sporomorph assemblages and relative percentage abundances of major taxa (i.e., Trees and shrubs, Herbs, Mosses and Ferns) recovered from the latest Eocene (35.50 Ma) to early-late Oligocene (27.46 Ma). A, G, and C are angiosperms, gymnosperms, and cryptogams, respectively. CONISS ordination constrains the latest Eocene to early-late Oligocene sporomorph assemblages into three main pollen zones (PZ 1-PZ 3), with PZ 2 divided into PZ 2a and PZ 2b. For components of the warm-temperate lowland and cool-temperate upland taxa, see Fig. 5.

with ±2σ. We refer to Willard et al. (2019) and Klages et al. (2020) for a more detailed explanation of the PDF method.

3. Results

The analysed late Eocene to late Oligocene samples from the western margin of Tasmania (ODP Site 1168) generally show good pollen recovery. 12 of the 51 samples analysed do not contain sufficient sporomorph counts and were not considered for further analyses. A total of 60 pollen taxa (including 11 gymnosperms and 34 angiosperms) and 15 spores were identified across the studied interval. The relative abundance and stratigraphic distribution of pollen taxa is shown in the pollen diagram (Fig. 2). The sporomorph record is dominated by *Nothofagidites* spp. (23–73%) and *Haloragacidites harrisii/Myricipites harrisii* (9–68%). *Podocarpidites* spp., *Cyathidites* spp., *Araucariacites*, and *Gleicheniidites* spp. form components of the sporomorph record occurring infrequently to moderately (<5%) during the Eocene but commonly in the Oligocene of Site 1168.

Average diversity for the entire section based on results from rarefaction is 14.0 ± 2.3 taxa/sample at 75 individuals. Based on results from CONISS analysis, the section is grouped into three main pollen zones (PZ; Fig. 2); PZ 1 (late Eocene; 35.50–34.81 Ma), PZ 2 (2a and 2b; latest Eocene to early Oligocene; 34.78–30.81 Ma) and PZ 3 (early to late Oligocene; 30.55–27.46 Ma).

3.1. Pollen Zone 1 (PZ 1; 35.50–34.81 Ma; 788.76–759.0 m b.s.f.; 6 samples)

PZ 1 is characterised by a high abundance of *Nothofagidites* spp. (*Nothofagus*; ~44%; Fig. 2) and *Myricipites harrisii* (*Gymnostoma*; ~40%). Within *Nothofagus*, taxa belonging to *brassii*-type (~28%) dominates, followed by the *fusca*-type (~13%), and *menzii*-type (~3%), respectively. Other angiosperms (non-*Nothofagus*) are dominated by *Myricipites harrisii* (~40%), with *Proteacidites* spp., *Periporopollenites polyoratus*, and *Spinizonocolpites* spp. (Arecaceae) being common across this zone. Gymnosperms (~10%) generally show low relative abundance and are represented in order of decreasing abundance by *Podocarpidites* spp., *Araucariacites australis* (Araucariaceae), *Phyllocladidites mawsonii* (*Lagarostrobos*), *Dacrydiumites praecupressinoides* (*Dacrydium*), and *Microcachryidites antarcticus* (*Microcachrys*). Cryptogams make up <5% of all non-reworked sporomorphs. The main components of this group, in order of decreasing abundance are *Cyathidites* spp., *Gleicheniidites* sp. (Gleicheniaceae), and *Cibotiidites tuberculiformis* (Schizaeaceae).

Quantitatively, PZ 1 is marked by relatively low number of sporomorph taxa and diversity. The average number of sporomorph taxa based on rarefaction is 12.97 ± 2.73 (mean ± SD) species per sample at 75 individuals (Table 1). Shannon diversity (H) and equitability (J) on average are 1.84 ± 0.37 and 0.72 ± 0.11 respectively (Fig. 3).

3.2. Pollen Zone 2 (PZ 2; 34.78–30.81 Ma; 757.46–719.0 m b.s.f.; 12 samples)

In PZ 2, the relative abundance of *Nothofagidites* spp. increases substantially in this zone and on average accounts for ~67% (Figs. 2 and 3) of all non-reworked sporomorph taxa. The *brassii*-type *Nothofagus* (~40%) still dominates, followed by the *fusca*-type (20%) and the *menzii*-type *Nothofagus* (4%). Other angiosperms (non-*Nothofagus*) are still dominated by *Myricipites harrisii* (*Gymnostoma*), however, there is a marked decline in their abundance from PZ 1 (~40%) to PZ 2 (~17%). *Proteacidites* spp., *Periporopollenites polyoratus*, and *Assamiapollenites inanis* are rare and occur sporadically across PZ 2. Another important observation is the gradual demise of *Spinizonocolpites* spp. (Arecaceae) in this zone. Gymnosperms represent the second most abundant group and account for ~12% of all non-reworked sporomorphs. These gymnosperms are represented by taxa (in order of decreasing abundance) *Podocarpidites* spp. (Podocarpaceae), *Araucariacites australis* (Araucariaceae), *Phyllocladidites mawsonii* (*Lagarostrobos*), and *Microcachryidites antarcticus* (*Microcachrys*). PZ 2 generally sees an increase in cryptogams, and they account for about 10% of all non-reworked sporomorphs. These are represented mainly by *Cyathidites* spp. (Cyatheaceae), *Gleicheniidites* spp. (Gleicheniaceae), and *Cibotiidites tuberculiformis* (Schizaeaceae).

Though PZ 2a and 2b generally show similarities in sporomorph content, subzone 2b (34.00–30.81 Ma) shows a decline of *Myricipites harrisii* (*Gymnostoma*), *Nothofagidites asperus* (*menzii*-type *Nothofagus*) and increase in *Cyathidites* spp. Although angiosperms such as *Proteacidites* sp., *Spinizonocolpites* spp., and *Malvacipollis subtilis* are minor components of subzone 2a, they are absent in subzone 2b. On the other hand, *Cibotiidites* (Schizaeaceae) occurs in subzone 2b, but not in subzone 2a. Based on results from rarefaction, sporomorph species for this zone on average is 12.78 ± 1.56 species per samples at 75 individuals and slightly lower than in PZ 1. Shannon diversity (H) and equitability (J) on average are 1.98 ± 0.19 and 0.78 ± 0.04 (Table 1; Fig. 3), respectively.

3.3. Pollen Zone 3 (PZ 3; 30.55–27.46 Ma; 701.30–547.30 m b.s.f.; 21 samples)

PZ 3 shows a notable increase in gymnosperms and cryptogams with a concomitant rise in sporomorph taxa diversity between 30.55 and 27.19 Ma (Oligocene). The average number of sporomorph taxa is 14.46 ± 1.41 species per sample at 75 individuals and is higher than PZ 1 and 2 (Table 1). Shannon diversity (H) and equitability (J) are on average 2.16 ± 0.15 and 0.81 ± 0.03 (Table 1; Fig. 3), respectively.

PZ 3 shows a significant decline in *Nothofagidites* spp. from a record peak of 67% in PZ 2 to ~43% in PZ 3. Pollen taxa belonging to the *brassii*-type *Nothofagus* continue to be dominant and account for ~33% of all non-reworked palynomorphs followed by the *fusca* and *menzii*-types accounting for 8% and 2%, respectively. Other angiosperms (non-*Nothofagus*) are still dominated by *Myricipites harrisii* (*Gymnostoma*), however, they show a slight recovery in relative abundance from their record low of ~17% in PZ 2 to ~22% in PZ 3. Additional non-*Nothofagus* angiosperms are rare and typically represented by one to three occurrences throughout this zone. These are *Proteacidites* spp. (Proteaceae), *Tricolpites* spp., *Gambierina rudata*, *Malvacipollis* spp. (Euphorbiaceae), *Microalatidites paleogenicus* (*Phyllocladus*), *Myrtaceidites* spp. (Myrtaceae), and *Sapotaceoidaepollenites latizonatus* (Sapotaceae). Gymnosperms in this zone show some increase in relative abundance from ~12% in PZ 2 to ~18% in PZ 3. *Podocarpidites* spp. (Podocarpaceae) and *Araucariacites australis* (Araucariaceae) reach their peak in this zone and account for ~8% and 7%, respectively, of all non-re-worked sporomorphs. Minor, but consistently present taxa include *Microcachryidites antarcticus* (*Microcachrys*), *Dacrydiumites praecupressinoides* (*Dacrydium*), *Dilwynites granulatus* (Araucariaceae), and *Phyllocladidites mawsonii* (*Lagarostrobos*). Cryptogams also show a significant rise in relative abundance and generally account for ~18% of all non-reworked sporomorphs. *Cyathidites* spp. (Cyatheaceae), and *Gleicheniidites* spp. (Gleicheniaceae) mark their peak occurrence in this zone and generally account for 8% and 7%, respectively, of all non-reworked sporomorphs. Other important components of this group, that occur in low numbers,

Table 1
Summary of species diversity from the late Eocene to early Oligocene of ODP Site 1168.

Analysis	Pollen Zone 1		Pollen Zone 2		Pollen Zone 3	
	Mean	*(SD)*	*Mean*	*(SD)*	*Mean*	*(SD)*
Rarefaction (75 individuals)	12.97	2.73	12.78	1.56	14.46	1.41
Rarefaction (100 individuals)	13.95	4.72	13.92	2.12	16.28	2.62
Shannon index (H)	1.84	0.37	1.98	0.19	2.16	0.15
Equitability (J)	0.72	0.11	0.78	0.04	0.81	0.03

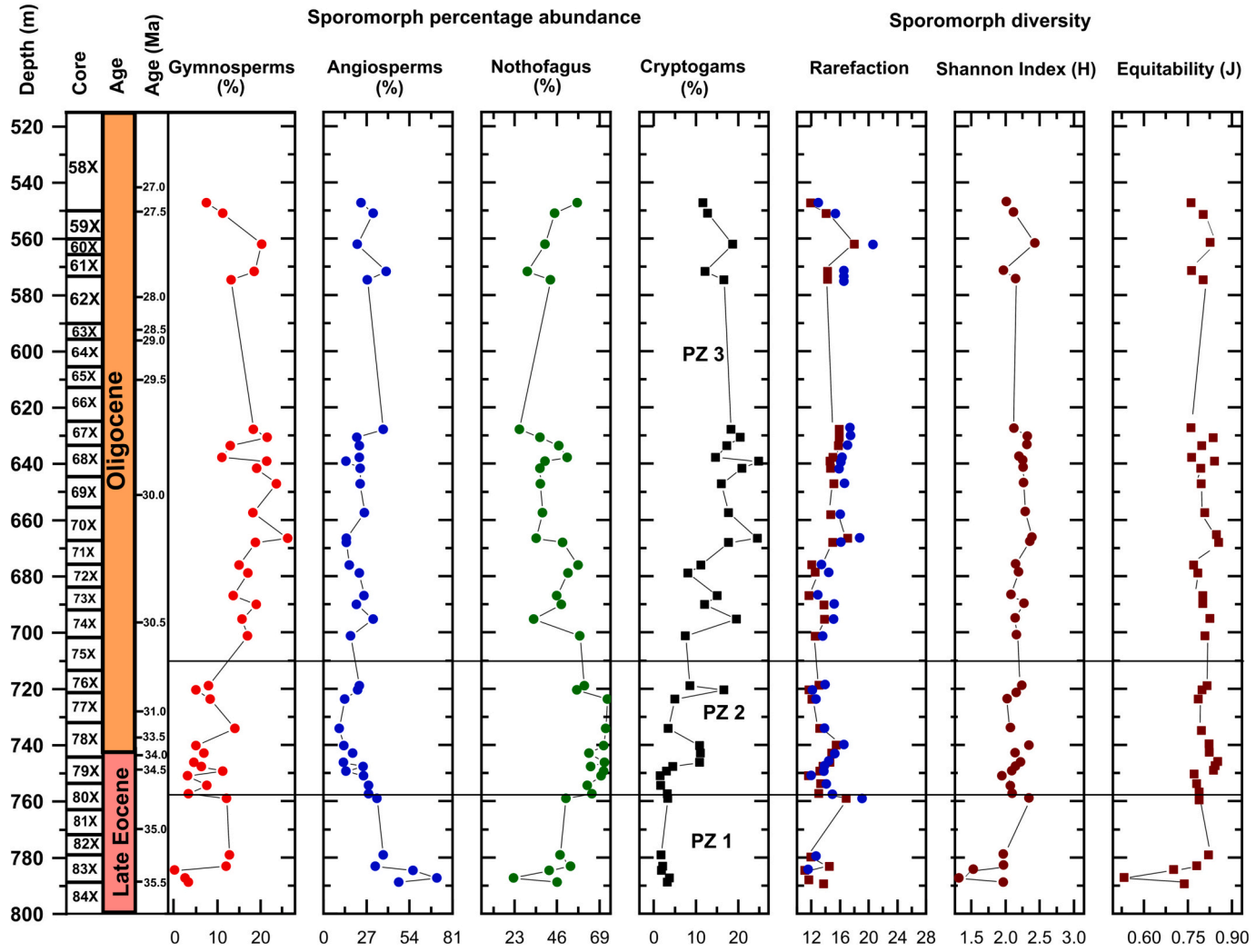

Fig. 3. Sporomorph percentage abundances and diversity indices for ODP Site 1168. Only samples with pollen counts ≥75 grains are presented and these are categorised into the main groups (angiosperms, gymnosperms, *Nothofagus* and cryptogams). Samples are rarefied at ≥75 and ≥ 100 individuals and have similar trends, however, only samples at ≥75 were used for calculation of diversity indices.

are *Osmundacidites* spp. (Osmundaceae), *Stereisporites antiquasporites* (Sphagnum/Sphagnaceae), *Polypodiisporites radiatus* (Polypodiaceae), *Clavifera* spp. (Gleicheniaceae), and *Baculatisporites comaumensis* (Hymenophyllaceae/*Hymenophyllum*).

3.4. Principal component analysis

The length of the first DCA axis (1.25 SD; Table 2) units indicates that species turnover changes linearly across the studied interval (time), making the application of PCA suitable for this data study.

The two main PCA axis account for 40.9% of the total variance. The first PCA axis explains 27.8% of the variance separating *Araucariacites-Gleicheniidites* from *Spinizonocolpites* spp.–*Proteacidites* sp., and providing evidence that these taxa thrive under different ecological and environmental conditions (Fig. 4). Based on the ecology of the NLRs represented by the encountered sporomorphs (see Supplementary Information Table S4; Amoo et al., 2022b), the first PCA axis (Dimension 1; Fig. 4) most likely represents a temperature gradient from relatively warm-temperate rainforests with thermophilic elements through to cool-temperate forests. This is represented by the separation of taxa such as *Spinizonocolpites* spp., *Proteacidites* sp., *Periporopollenites polyoratus*, and *Proteacidites pachypolus* with negative sample scores, most likely indicating warm-temperate lowland habitats, and positive sample scores for *Araucariacites*, *Podocarpidites* sp., *Microcachryidites antarcticus*, and *Gleicheniidites* possibly suggesting cool-temperate climate conditions with MATs between 6 and 12 °C (Emanuel et al., 1985).

Table 2
Total variance (eigenvalue) and axis lengths indicated by the first four DCA components of the pollen data set from ODP Site 1168.

	DCA1	DCA2	DCA3	DCA4
Eigenvalues	0.132	0.080	0.023	0.022
Axis lengths	1.248	1.272	0.644	0.600

4. Discussion

4.1. Warm temperate forest versus cool temperate forest taxa

The varying percentages of cool-temperate and thermophilic taxa (Fig. 4), suggest that the vegetation across the studied time interval in western Tasmania was subject to temporal changes in temperature. However, the co-occurence of different vegetation communities with different climate envelopes also suggest that vegetation across Tasmania were subject to a spatial climatic gradient related to differences in elevation and/or distance to the coastline. This is supported by reports of a topographic divide between sites facing the cool Tasman current

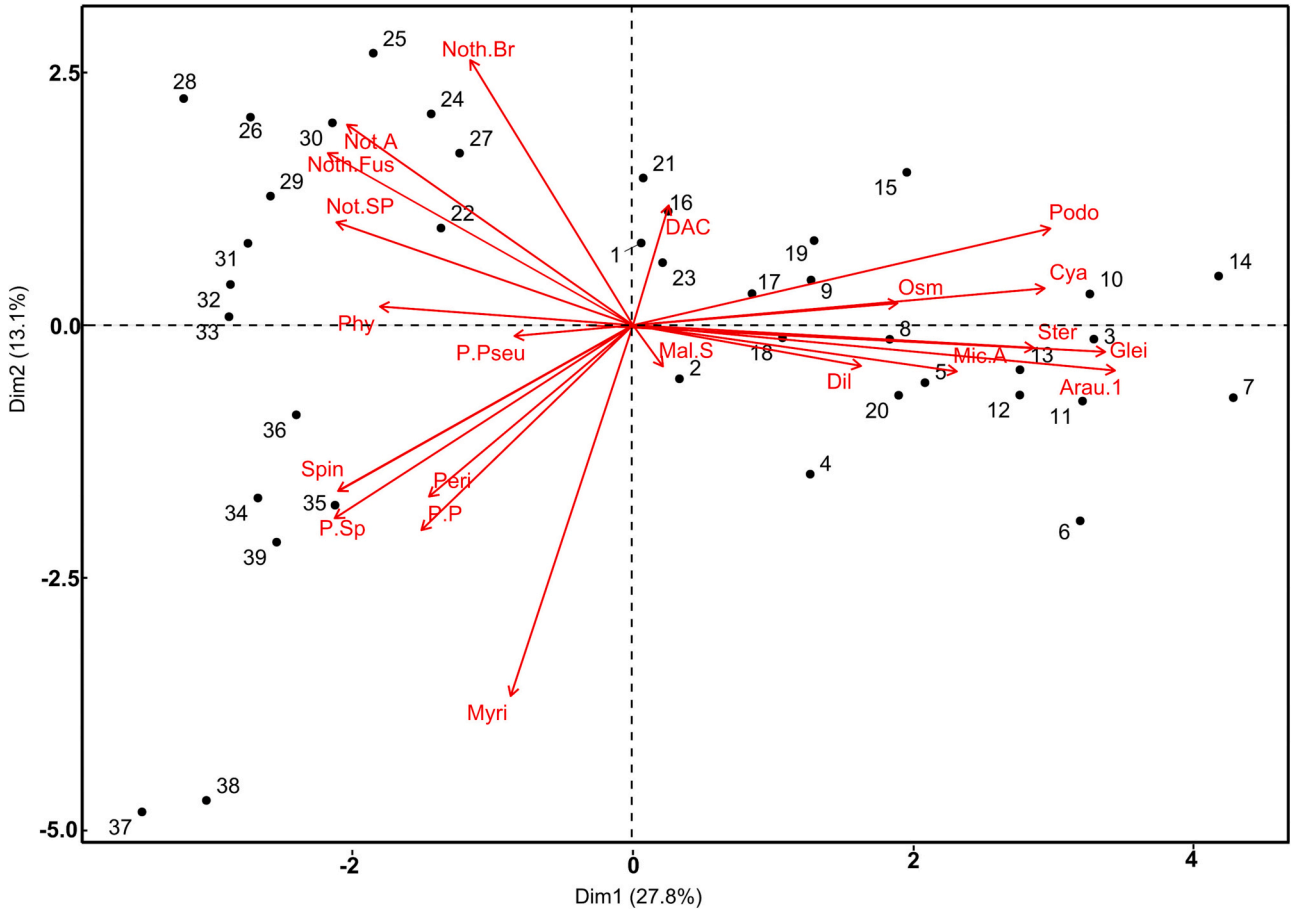

Fig. 4. PCA biplot of western Tasmania pollen data showing the scores for the main pollen types. The main PCA axis (Dim 1) coupled with knowledge of the ecological preference of these taxa show a shift in latitudinal gradient from a lowland habitat through to upland conditions. Numbers from 1 to 39 represent sample IDs, with 39 being the oldest (35.50 Ma) and 1 being the youngest (27.46 Ma). Taxa are explained as follows; Myri = *Myricipites harrisii*, P·P = *Proteacidites pachypolus*, Peri = *Periporopollenites*, Spini = *Spinizonocolpites* spp., P. Sp = *Proteacidites* sp., P. pseu = *Proteacidites pseudomoides*, Phy = *Phyllocladidites mawsonii*, Not. Sp = *Nothofagidites* spp., Noth. Fus = *Nothofagidites fuscospora*, Not. A = *Nothofagidites asperus*, Noth.Br = *Nothofagidites brassospora*, DAC = *Dacrydiumites*, Podo = *Podocarpidites*, Osm = *Osmundacidites*, Cya = *Cyathidites*, Ster = *Stereisporites*, Glei = *Gleicheniidites*, Mic.A = *Microcachryidites antarcticus*, Mal.S = *Malvacipollis subtilis*, Dil = *Dilwynites*, Arau = *Araucariacites australis*.

(Gippsland basin, eastern Tasmania) and the westerly located south Australian basins (Holdgate et al., 2017) that may have served as the location for higher altitude temperate forest taxa. Abundant *Nothofagidites* spp. (especially *brassii*-type *Nothofagus*), with *Myricipites harrisii*, and common *Phyllocladidites mawsonii* give an indication of *Nothofagus-Gymnostoma* dominated warm-temperate temperate rainforest (Figs. 2 and 5) thriving under high precipitation regimes (MAP >1400 mm/yr) in western Tasmania during the late Eocene. In addition, pollen taxa belonging to Arecaceae and *Proteacidites pseudomoides*, indicate the existence of thermophilic elements between 35.50 and 34.81 Ma that most likely occupied the warmer sheltered lowlands and coastal areas (Huurdeman et al., 2021; Amoo et al., 2022a). The two possible NLR relatives for *Proteacidites pseudomoides* are *Carnarvonia* and *Lomatia*. *Carnarvonia* thrives in warm temperate to tropical areas such as wet northeastern Australia (Cooper and Cooper, 2004) whereas *Lomatia* grows as shrubs and small trees in remnant gallery warm temperate rainforests (Bowman et al., 2014; Myerscough et al., 2007). *Carnarvonia* is selected as the likely NLR based of the PCA grouping with other thermophilic taxa (Fig. 4). This is also in agreement with comparable studies in the southern high latitude (e.g., Bowman et al., 2014; Amoo et al., 2022a; Sluiter et al., 2022).

The early to late Oligocene (~30.4–27.46 Ma) is characterised by a shift from warm-temperate to cool-temperate forests, evidenced by increases in occurrence of taxa such as Araucariaceae, *Microcachrys*, and *Sphagnum* (peat moss) and the regular occurrence (<5%) of the Proteaceae *Bellendena montana* (Figs. 2 and 5). These taxa represent a component of the palynoflora record that today occupy cool temperate habitats with more open vegetation growing in low nutrient, but well-drained soils (Macphail et al., 1999; Kershaw and Wagstaff, 2001; Bowman et al., 2014). Extant members of *Araucariaceae* are tall trees generally confined to the lower mid-latitudes (Kershaw and Wagstaff, 2001). However, in our PCA biplot and pollen diagram, *Araucariaceae* is associated with other cool-temperate taxa, making an affinity with the extant cool-temperate monkey puzzle tree (*Araucaria araucana*) more likely (Sanguinetti and Kitzberger, 2008; Bowman et al., 2014; Contreras et al., 2014). The community includes *Bellendena montana* (NLR of *Proteacidites parvus*), *Microcachrys*, and shrubs of *Nothofagus* subgenera *Fuscospora* and *Lophozonia* (e.g., Anker et al., 2001), as well as scrubs of *Gymnostoma* and *Dacrydium* (e.g. in New Caledonia; Hope, 1996), and *Sphagnum* (e.g., in Tasmania and Australia; Seppelt, 2006). The increasing expansion of *Sphagnum* moss across this section (~30.4–27.46 Ma) may indicate the expansion of boggy habitats during a period of cooling (Panitz et al., 2016).

Nothofagus subgenus *Brassospora* could not be grouped under the typical warm temperate or cool temperate vegetation. Today, the *Brassopora*-type *Nothofagus* are found thriving in temperate to subtropical climate conditions in New Guinea and New Caledonia (Read et al., 2005). This *Brassospora*-type *Nothofagus* grows today at lower to mid

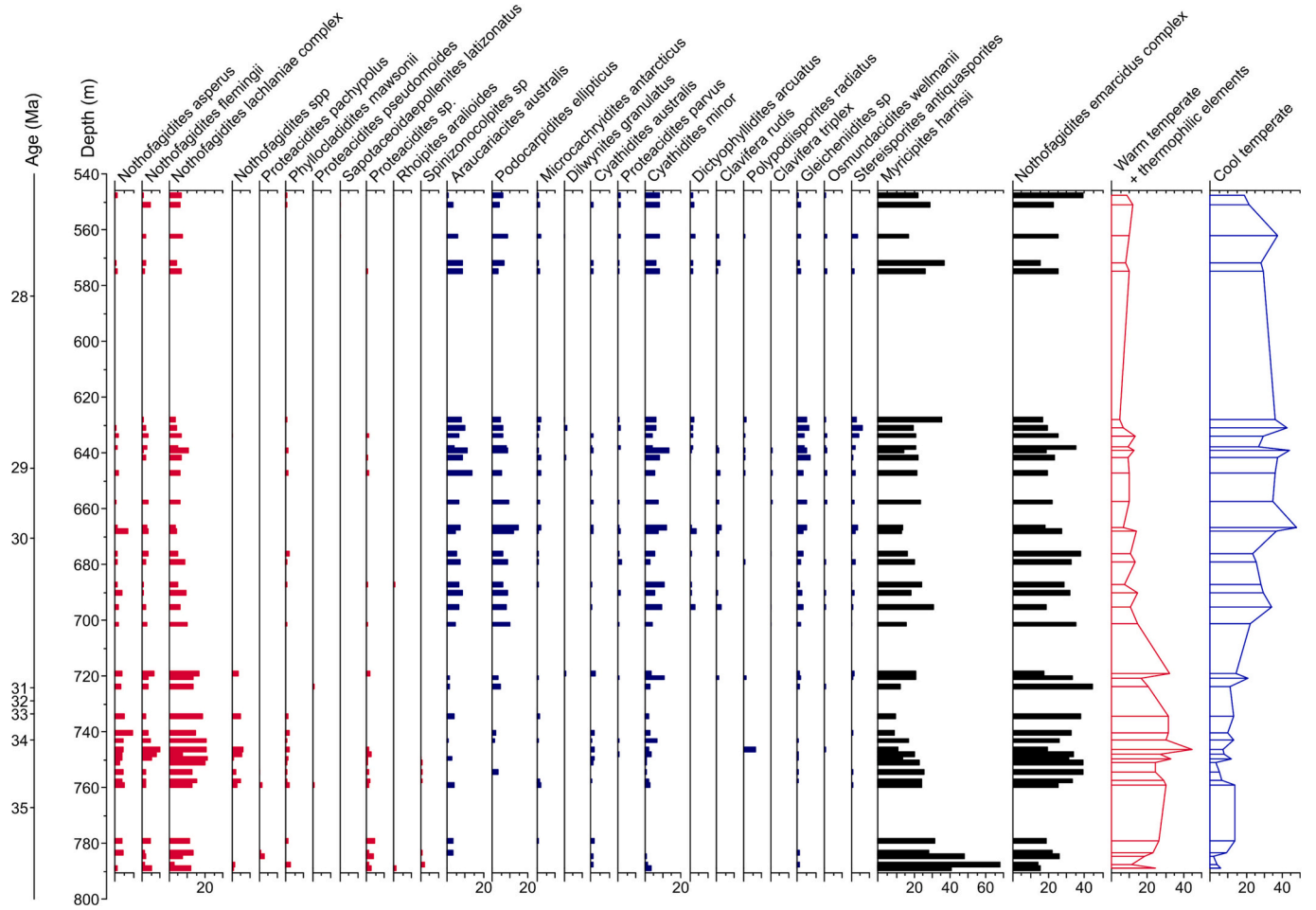

Fig. 5. Relative abundance of main sporomorphs groups. Red bars indicate taxa whose NLRs are today mostly found thriving in warm-temperate to subtropical lowland habitats, blue bars indicate taxa whose NLRs are found thriving in cool-temperate uplands areas, and black bars represent taxa that dominant the whole section and could thrive in both warm and cool-temperate environments. (For interpretation of the references to colour in this figure legend, the reader is referred to the web version of this article.)

altitudes that receive high and consistent rainfall, as well as in montane and subalpine areas (typically above 500 m a.s.l), pointing to their wide ecological and climatic tolerance (MAT: 10.6 to 23.5 °C; Read et al., 2005). *Gymnostoma*, on the other hand are tropical to subtropical rainforest trees that can grow up to 12 m in open, sunny gaps from riparian (along riverbanks) niches to mountain top situations (altitudes between 200 and 1000 m a.s.l), and are today mostly found in the Malesian-Australian region and New Caledonia (Hope, 1996; Prider and Christophel, 2000; Steane et al., 2003; Korasidis et al., 2019). Though *Myricipites harrisii* (Casuarinaceae) has two potential NLRs, *Casuarina/Allocasuarina* and *Gymnostoma*, the rainforest clade *Gymnostoma* is selected as the most likely NLR. This is deduced from the associated species during the late Eocene of our study site, which is mostly dominated by rainforest taxa. This interpretation is supported by previous southern Australian Paleogene studies suggesting that the rainforest clade, *Gymnostoma* dominated throughout the Eocene and Oligocene (Hill, 2017; Lee et al., 2016), only to be replaced by the sclerophyllous/xeromorphic clade *Casuarina/Allocasuarina* in the Miocene (Hill and Scriven, 1995; Boland et al., 2006; Holdgate et al., 2017).

4.2. Latest Eocene warm-temperate climate and vegetation from 35.50 to 34.81 Ma

Throughout the PZ 1 assemblage (PZ 1; 35.50–34.81 Ma), abundant *Nothofagus* spp., with secondary *Gymnostoma*, and minor angiosperm (*Carnarvonia*, Arecaceae, Proteaceae) suggest the presence of a temperate *Nothofagus*-dominated rainforest with subtropical elements, growing under MATs ~13 °C and MAPs between 1483 and 1892 mm/yr (Fig. 6) in western Tasmania. The presence of minor components of cool-temperate taxa such as *Microcachrys*, Podocarpaceae, and Araucariaceae suggest input or transport from high-altitude cool temperate forests. The occurrence of warmth-loving (mesothermal) taxa such as Arecaceae, *Carnarvonia*, Myrtaceae, *Gymnostoma*, and Proteaceae in this zone, suggests the presence of a temperate-thermophilic vegetation community. There is also a distinct cluster of taxa along the second PCA axis (Dim 2; Fig. 4) with all groups of *Nothofagus* assembled in one area (positive scores), and taxa such as *Carnarvonia*, Arecaceae, Proteaceae, Trimeniaceae, and *Gymnostoma* on the other end (negative scores), suggesting a separation of a more diverse coastal forest from an inland *Nothofagus*-dominated forest. Based on the habitat of their NLRs, thermophilic element such as Arecaceae are considered to have occupied sheltered lowland and coastal areas requiring relatively milder/non-freezing winter temperatures, due to their sensitivity to frost (Larcher and Winter, 1981; Tomlinson, 2006; Reichgelt et al., 2018). Apart from one sample at ~35.27 Ma which records a MAT of 11 °C (Fig. 6), all the other samples in this zone yield sporomorph-based MATs above 12 °C indicating that the climate phase in this zone is predominantly warm-temperate (Emanuel et al., 1985). The warm-temperate climate at western Tasmania is comparable to the biomarker based (brGDGT) reconstructions of warm climates at Prydz Bay between 37.7 and 34.7 Ma (Tibbett et al., 2021). In eastern Tasmania, there is a fluctuation between warm-and-cool temperate climate between 35.50 and 34.59 Ma

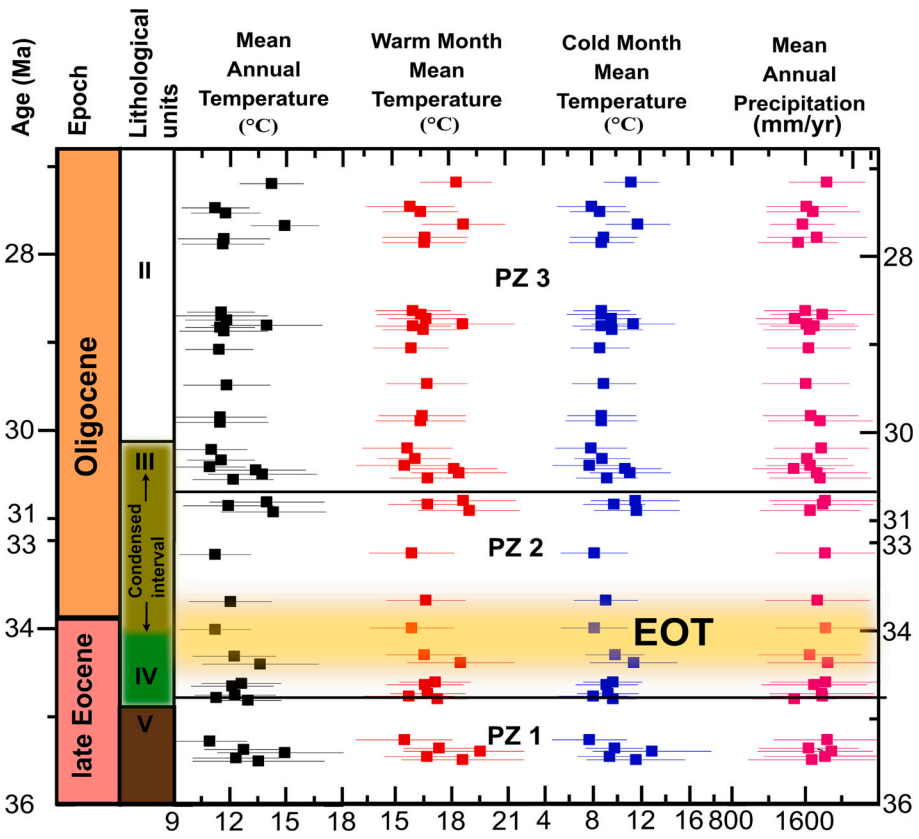

Fig. 6. Climate estimations based on sporomorphs utilising probability density functions (PDFs). Mean annual temperature (MAT), warm month mean temperature (WMMT), cold month mean temperature (CMMT), and mean annual precipitation (MAP) are shown from left to right. The climate estimates are reported as the mean value±2SD. The quantitative temperature estimations are given in degrees Celsius, while MAP is given in millimetres per year. The wiggle line between 33 and 31 Ma indicates a sediment hiatus.

(Amoo et al., 2022a), which has been linked to the initial deepening and widening of the Tasmanian gateway that caused eastern Tasmania to come under the influence of the warm PLC (Stickley et al., 2004; Hoem et al., 2021). Mesothermic conditions are reported for the late Eocene of southeast Australia from sporomorph-based MATs reconstructed between 12 and 20 °C (Pound and Salzmann, 2017), 14–22 °C (Korasidis et al., 2019) and 15–20 °C (Sluiter et al., 2022; Fig. 7), and terrestrial biomarkers (Lauretano et al., 2021).

4.3. Progression towards cooler climate conditions across the EOT (~34.46–33.69 Ma) and rebound in the earliest Oligocene (33.15–30.81 Ma)

PZ 2 ultimately captures the EOT and post-EOT (earliest Oligocene). The sporomorph-based MATs at the EOT provide evidence for a cooling of ~2 °C between 34.46 and 33.69 Ma in western Tasmania (Fig. 6). Although this estimated cooling appears to be only minor and with overlapping error ranges, a shift in the abundance of several taxa at the onset of the EOT provide additional evidence for a major change in vegetation cover in response to cooling. As our bioclimate analysis uses presence/absence of taxa only, these changes in pollen percentages are not captured in our quantitatively estimated temperature. Percentage change include a sharp increase in *Nothofagus* (Fig. 3) along with a decline of the thermophilic *Gymnostoma*. A slight increase in *Nothofagus* subgenera *Lophozonia* and *Fuscospora* generally supports the interpretation of a brief cold interval across the EOT. The cooling at the EOT also led to the demise of Arecaceae (NLR of *Spinizonocolpites* spp.), a drop in angiosperms (non-*Nothofagus*), and slight increase in cryptogams (Fig. 3). Previous studies in southern Australia (e.g., Macphail et al., 1994; Benbow et al., 1995; Macphail, 2007; Holdgate et al., 2017; Korasidis et al., 2019; Lauretano et al., 2021) and eastern Tasmania (Amoo et al., 2022a) reported the concurrent demise of diverse angiosperm flora including members of the Proteaceae, a sharp rise in *Nothofagus* and decline and demise of megathermal taxa attributed to increasingly cooler climate conditions (Martin, 1994; Partridge and Dettmann, 2003). In New Zealand, the increase in relative abundance of *Nothofagus* in the late Eocene and across the EOT has also been attributed to the onset of the EOT cooling (Pocknall, 1989; Prebble et al., 2021), in agreement with our interpretation for western Tasmania. This terrestrial cooling across the EOT matches regional and global temperature records) and is generally linked to a global decline in atmospheric pCO_2 (Colwyn and Hren, 2019; Korasidis et al., 2019; Lauretano et al., 2021; Tibbett et al., 2021). The equatorward movement of the Australian continent may have mitigated the cooling caused by declining pCO_2 across the EOT. The appearance, and in some instances, the increase in fern spores (Cyatheaceae, Gleicheniaceae, and Schizaeaceae) gives an indication of an environmental disturbance resulting in cooling across this zone. The cooling and associated decline of the warmth-adapted taxa may have created gaps in the canopy and/or expansion of boggy habitats that were then occupied by ferns (Thompson et al., 2022).

The interval between ~33.69 and 33.15 Ma captures the early Oligocene glacial maximum (EOGM; Liu et al., 2009; Hutchinson et al., 2021). This interval is generally correlative with the normal magnetic polarity C13n (33.705–33.157 Ma; Gradstein et al., 2012) of the early Oligocene. The sporomorph-based climate estimates indicate cool-temperate climate conditions with MATs between 11.2 and 12 °C (Fig. 6). In addition, the dominance of *Nothofagus* (*Brassospora* and *Fuscospora*) and consistent occurrence of *Lagarostrobos* and *Microcachrys*, indicate a period of sustained cool-temperate conditions. Today, in New Zealand, Tasmania, and southern Australia, *Nothofagus* (*fusca*-type) dominates cool-temperate vegetation (Kershaw, 1988). The interval of sustained cool-temperate conditions is comparable to the earliest Oligocene estimates from the Gippsland Basin in southeast Australia (Korasidis et al., 2019) and the earliest Oligocene of eastern Tasmania (Amoo et al., 2022a). The relatively low resolution of Site 1168 EOGM record in comparison to Site 1172 is compensated by the longer post-EOT (early Oligocene) record available for this study. Whereas climate estimates for Site 1172 indicate a post-EOT warming phase between

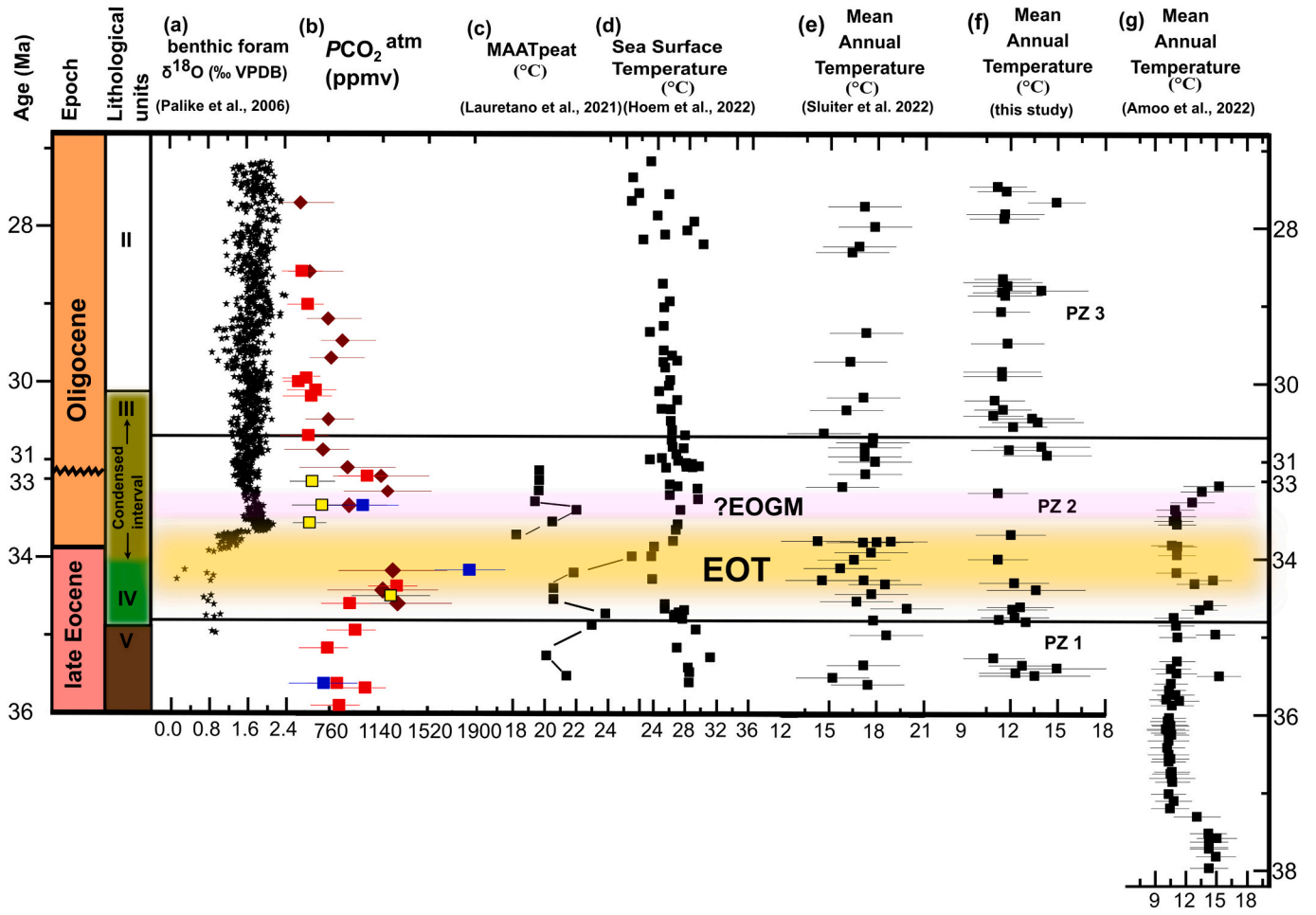

Fig. 7. Comparison of the sporomorph-based MATs in the Tasmanian Gateway region across the EOT and post-EOT global marine EOT and early Oligocene records. (a) benthic foraminiferal $\delta^{18}O$ record from ODP 1218 (Pälike et al., 2006). (b) Marine δ11 B-derived atmospheric pCO_2 record (brown kite-like symbol with error bars; Anagnostou et al., 2016); Alkenone-based pCO_2 estimates derived from haptophyte algae for Site 516 and 612 (Pagani et al., 2005; data points are red boxes with error bars); Refined Alkenone-based pCO_2 estimates for ODP Sites 277 and 511 (black and yellow boxes, respectively; Zhang et al., 2020). (c) MBT'5me-based MAATsoil (Lauretano et al., 2021). (d)TEX_{86}-derived Sea surface temperature from ODP site 1168 (SST; Hoem et al., 2022). (e) Sporomorph-based quantitative MATs of the Gippsland Basin (Sluiter et al., 2022). (f) Sporomorph-based quantitative from ODP Site 1168 (this study). (g) sporomorph-based MATs from ODP site 1172 (Amoo et al., 2022a). Wiggle line between ~33 and 31 Ma indicates sediment hiatus. (For interpretation of the references to colour in this figure legend, the reader is referred to the web version of this article.)

~33.25 to 33.06 Ma, our record from Site 1168 gives an indication that at least in western Tasmania, the post-EOT warming phase extended and reached ~30.44 Ma (base of PZ 3) with an average quantitative sporomorph-based MAT estimate of ~13 °C (Fig. 6). On a regional scale, other studies from southern Australia (Korasidis et al., 2019; Sluiter et al., 2022) show similar cooling across the EOT but with disparate climate trends post-EOT (early Oligocene). Korasidis et al. (2019) reported a monotonous cooling trend from mesothermic/warm-temperate climate conditions in the late Eocene to a microthermic/cool-temperate climate phase across the EOT and the early Oligocene. Whereas Sluiter et al. (2022) provided evidence to support a cooling trend across the EOT, with a return to mesothermal conditions (warming) in the early Oligocene (post-EOT; Fig. 7). Though our MAT records across the EOT and early Oligocene (~30.4 Ma) show a general agreement in trends, the Gippsland Basin MATs (Sluiter et al., 2022) are generally 2–4 °C higher than western Tasmania. This could be due to latitudinal differences between these sites (Gippsland Basin was ~5°N of western Tasmania during the late Eocene and early Oligocene). The terrestrial cooling across the EOT and transient warming in the earliest Oligocene of Site 1172 were linked to the decline in concentration of atmospheric carbon dioxide (pCO_2) and its recovery (Amoo et al., 2022a). However, the Site 1168 sporomorph-based MAT records indicate that the composite post-EOT warm-temperate phase extended well into the early Oligocene at ~30.44 Ma, which matches the general sporomorph-based MAT trend in southeast Australia (Sluiter et al., 2022). There is a general match between the Site 1172 MATs and pCO_2 post-EOT. However, the temperature change at Site 1168 during the warm-temperate post-EOT phase from ~33.0 to ~30.4 Ma appears to be decoupled from the global pCO_2 trend (Fig. 7).

Reconstructed SSTs indicate a ~ 4 °C cooling (from ~27 to ~23 °C) at the onset of the EOT followed by a recovery to relatively high temperatures comparable to pre-EOT levels until ~30 Ma (Fig. 7; Hoem et al., 2022). The marine-based temperature trends match our terrestrial sporomorph-based MATs (~10–15 °C) although absolute temperatures are significantly lower (Fig. 7). This is most likely due to a warm bias in the TEX_{86} temperature proxy (Naafs et al., 2017; Hartman et al., 2018). Model simulations (Sauermilch et al., 2021) and palaeoceanographic reconstructions (Stickley et al., 2004; Hoem et al., 2021) point to the interval across the EOT and until ~30.2 Ma being characterised by condensed sedimentary section and a series of hiatuses. These hiatuses are due to increased sediment transport from ocean currents associated with bottom-water activity in the Tasmanian Gateway region. The records are reported to have carried no evidence for a decrease in SST, but rather by ~30.2 Ma, a stable, deep-marine setting consistently

influenced by relatively warm waters had been established (Stickley et al., 2004; Hoem et al., 2021). This therefore shows that, aside from the decline of pCO_2 across the EOT and its transient recovery in the earliest Oligocene, other forcing(s) may have been responsible for the relatively sustained warm terrestrial climate phase in this region until ~30.4 Ma. The plausible driver for this phenomenon is most likely a relatively local forcing (e.g., the sustained deepening of the Tasmanian Gateway) that acts in conjunction with a more global driver such as changes in atmospheric pCO_2.

4.4. Establishment of a cool-temperate vegetation and climate in the early to late Oligocene (30.4–27.46 Ma)

Despite the evidence for a warm-temperate post-EOT climate extending into the lower sections of PZ 3 (~30.4 Ma), the terrestrial palynomorph assemblage from western Tasmania (Site 1168) does not indicate any major change in vegetation composition until after ~30.4 Ma. The interval between 30.4 and 27.46 Ma is characterised by an expansion of cryptogams and coniferous taxa such as Araucariaceae, *Podocarpus*, *Dacrydium*, and *Microcachrys* indicating an expansion of cool-temperate vegetation. The Shannon diversity index shows that the early Oligocene cool-temperate forest was more diverse in comparison to the latest Eocene vegetation (Table 1). This interpretation agrees with the earliest Oligocene *Nothofagus*-dominated rainforest in the Drake Passage area (Thompson et al., 2022). Previous early Oligocene studies in Antarctica (Cantrill, 2001; Raine and Askin, 2001; Prebble et al., 2006; Griener and Warny, 2015) indicate a decline in taxa diversity due to significant cooling and drying, which ultimately resulted in the *Nothofagus-Podocarpus* vegetation taking on a low-stature and shrubby form. However, considering the higher diversity of taxa in this interval, increases in relative abundance of non-*Nothofagus* angiosperms (especially *Gymnostoma*), and cryptogams, the *Nothofagus*-dominated rainforest with secondary *Gymnostoma* is most likely to have been intermediate in stature, with openings or gaps that would have been occupied by ferns, mosses, and shrubs (Macphail et al., 1994). This interpretation is further supported by the increase in *Sphagnum* mosses (*Stereisporites*) in this interval. *Sphagnum* mosses have been reported to represent cold tundra vegetation in various Oligocene records from Antarctica, Tasmania, and southeast Australia (Askin and Raine, 2000; Prebble et al., 2006; Amoo et al., 2022a; Sluiter et al., 2022; Thompson et al., 2022). Today, in Australia and Tasmania, they typically grow in carpet-like fashion colonising nutrient-poor acidic wetlands in cool temperate alpine-subalpine communities (Seppelt, 2006). Within this same interval of the early Oligocene, sporomorph-based quantitative estimates reveal generally cool-temperate climates with average MATs ~11 °C. However, the scattered occurrence of thermophilic taxa, such as *Beauprea*, Myrtaceae, and Sapotaceae, (e.g., at 27.68 and 28.80 Ma), suggest that pockets of warm temperate vegetation may still have survived in sheltered locations.

Palaeoceanographic reconstructions suggest a stable deep-marine setting with relatively warm surface waters associated with the PLC continued into the earliest Oligocene (Stickley et al., 2004). Except for a brief interval around ~28 Ma, the SST reconstructions generally show a cooling trend in this region after ~31 Ma (Hoem et al., 2022). This general cooling trend agrees with the sustained cool-temperate climate conditions in our terrestrial records and further matches the general trend of declining pCO_2 concentrations in the early Oligocene (Fig. 7). The correspondence between temperature (SST gradual decline; Hoem et al., 2022) and atmospheric pCO_2 most likely indicates the coupling of ocean-atmosphere system and the role of pCO_2 in driving terrestrial climate and vegetation change in the Tasmanian Gateway region.

5. Conclusions

This study presents a new sporomorph record from ODP Site 1168 to reconstruct vegetation and climate dynamics of Tasmania during the late Eocene (35.50 Ma) to Oligocene (27.46 Ma). The sporomorph record across the studied interval is characterised by three main pollen zones (PZ 1, PZ 2, and PZ 3). The latest Eocene PZ 1 (35.50–34.81 Ma) is characterised by a warm-temperate *Nothofagus* (dominated by the *brassii*-type) rainforest with thermophilic elements and a sporomorph-derived MAT ~13 °C. The sporomorph assemblage in this interval is comparable to the latest Eocene PZ 3 of Site 1172 interpreted to mark the stage of the initial deepening of the Tasmanian Gateway. PZ 2 (34.4–30.5 Ma) is characterised by a ~ 2 °C terrestrial MAT decline across the EOT (34.40–33.65 Ma) and an extended period of warm-temperate conditions post-EOT. However, the relatively extended post-EOT warming results in a mismatch between pCO_2 and terrestrial temperatures after ~33 Ma, suggesting that there may be factors aside from greenhouse forcing that contributed to this phenomenon. One explanation could be the equatorward movement of the Australian landmass, but it is more likely to be the influence of the PLC - a warm-water oceanic current. Deepening of the Tasmanian Gateway during this interval led to the establishment of a stable deep-marine setting and warm surface water associated with the PLC. This partial decoupling from the global climate by a regional warm-water current was only observed in PZ 2. Our *Nothofagus*-dominated temperate forest did not see any dramatic change in composition until after 30.5 Ma (PZ 3). During PZ 3 there is an observed increase in gymnosperms (notably Araucariaceae), cryptogams, and angiosperms, coupled with a slight increase in taxa diversity. The expansion of a cool-temperate forest further matches the general trend of declining pCO_2 concentrations in the early Oligocene. The early Oligocene (30.40–27.46 Ma) synchroneity between temperature (SST gradual decline and MATs) and atmospheric pCO_2 most likely indicate the coupling of the ocean-atmosphere system in the southern Australian region, and the role of pCO_2 in driving terrestrial climate and vegetation change onshore Tasmania. Our study provides evidence for the importance of both tectonic and pCO_2 forcing on vegetation and climate in the Tasmanian region during the late Eocene to Oligocene.

Declaration of Competing Interest

The contact author has declared that neither they nor their co-authors have any competing interests.

Data availability

All data are available on the Zenodo online data repository at https://doi.org/10.5281/zenodo.7902416

Acknowledgements

Samples for this study were supplied by the Ocean Drilling Program (ODP) sponsored by the US National Science Foundation under the management of the Joint Oceanographic institutions (JOI). Sefa Sahin is thanked for providing support with the multivariate statistical techniques. Michael Amoo acknowledges financial support from the Northumbria University Research Development Fund (RDF). Nick Thompson received funding from the Natural Environment Research Council (NERC)-funded Doctoral Training Partnership ONE Planet [NE/S007512/1]. Peter K. Bijl acknowledges funding from the European Research Council for starting grant number 802835, OceaNice. Frida S. Hoem acknowledges funding from Dutch research council (NWO) Polar Programme (grant no. ALW.2016.001).

Appendix A. Supplementary data

Supplementary data to this article can be found online at https://doi.org/10.1016/j.palaeo.2023.111632.

References

Amoo, M., Salzmann, U., Pound, M.J., Thompson, N., Bijl, P.K., 2022a. Eocene to Oligocene vegetation and climate in the Tasmanian Gateway region were controlled by changes in ocean currents and pCO2. Clim. Past 18, 525–546. https://doi.org/10.5194/cp-18-525-2022.

Amoo, M., Salzmann, U., Pound, M., Hoem, F.S., Thompson, N., Bijl, P.K., 2022b. Dataset for terrestrial climate and vegetation change in the western Tasmanian region from the late Eocene to late Oligocene. Zenodo [Data set]. https://doi.org/10.5281/zenodo.7902416.

Anagnostou, E., John, E.H., Edgar, K.M., Foster, G.L., Ridgwell, A., Inglis, G.N., Pancost, R.D., Lunt, D.J., Pearson, P.N., 2016. Changing atmospheric CO2 concentration was the primary driver of early Cenozoic climate. Nature 533, 380–384. https://doi.org/10.1038/nature17423.

Anker, S.A., Colhoun, E.A., Barton, C.E., Peterson, M., Barbetti, M., 2001. Holocene vegetation and paleoclimatic and paleomagnetic history from Lake Johnston, Tasmania. Quat. Res. 56, 264–274. https://doi.org/10.1006/qres.2001.2233.

Askin, R.A., Raine, J.I., 2000. Oligocene and Early miocene terrestrial palynology of the cape roberts drillhole CRP-2/2A, Victoria Land Basin, Antarctica. Terra Antarct. 7, 493–501.

Benbow, M.C., Alley, N.F., Callan, R.A., Greenwood, D.R., 1995. In: Dexel, J.F., Preiss, W. V. (Eds.), Geological History and Palaeoclimate, pp. 208–217. Adelaide.

Bijl, P.K., Houben, A.J.P., Hartman, J.D., Pross, J., Salabarnada, A., Escutia, C., Sangiorgi, F., 2018. Paleoceanography and ice sheet variability offshore Wilkes Land, Antarctica – Part 2: Insights from Oligocene–Miocene dinoflagellate cyst assemblages. Clim. Past 14, 1015–1033. https://doi.org/10.5194/cp-14-1015-2018.

Bijl, P.K., Frieling, J., Cramwinckel, M.J., Boschman, C., Sluijs, A., Peterse, F., 2021. Maastrichtian–Rupelian paleoclimates in the southwest Pacific – a critical re-evaluation of biomarker paleothermometry and dinoflagellate cyst paleoecology at Ocean Drilling Program Site 1172. Clim. Past 17, 2393–2425. https://doi.org/10.5194/cp-17-2393-2021.

Birks, H.J.B., Line, J.M., 1992. The use of rarefaction analysis for estimating palynological richness from Quaternary pollen-analytical data. The Holocene 2, 1–10. https://doi.org/10.1177/095968369200200101.

Birks, H.J.B., Felde, V.A., Bjune, A.E., Grytnes, J.A., Seppä, H., Giesecke, T., 2016. Does pollen-assemblage richness reflect floristic richness? A review of recent developments and future challenges. Rev. Palaeobot. Palynol. 228, 1–25. https://doi.org/10.1016/j.revpalbo.2015.12.011.

Boland, D., Brooker, M., Chippendale, G., Hall, N., Hyland, B., Johnston, R., Kleinig, D., McDonald, M., Turner, J., 2006. Forest Trees of Australia, 5th ed. CSIRO, Melbourne.

Bowman, V.C., Francis, J.E., Askin, R.A., Riding, J.B., Swindles, G.T., 2014. Latest Cretaceous-earliest Paleogene vegetation and climate change at the high southern latitudes: palynological evidence from Seymour Island, Antarctic Peninsula. Palaeogeogr. Palaeoclimatol. Palaeoecol. 408, 26–47. https://doi.org/10.1016/j.palaeo.2014.04.018.

Brinkhuis, H., Sengers, S., Sluijs, A., Warnaar, J., Williams, G.L., 2003. Latest Cretaceous–Earliest Oligocene and Quaternary Dinoflagellate Cysts, ODP Site 1172, East Tasman Plateau. In: Proceedings of the Ocean Drilling Program, 189 Scientific Results. https://doi.org/10.2973/odp.proc.sr.189.106.2003.

Cande, S.C., Stock, J.M., 2004. Cenozoic reconstruction of the Australia-New Zealand-south Pacific sector of Antarctica. In: Geophysical Monograph Series. American Geophysical Union, pp. 5–18.

Cantrill, D.J., 2001. Early Oligocene Nothofagus from CRP-3, Antarctica: implications for the vegetation history. Terra Antart. 8, 401–406.

Cavalli-Sforza, L.L., Edwards, A.W., 1967. Phylogentic analysis. Am. J. Hum. Genet. 19, 233–257.

Colwyn, D.A., Hren, M.T., 2019. An abrupt decrease in Southern Hemisphere terrestrial temperature during the Eocene–Oligocene transition. Earth Planet. Sci. Lett. 512, 227–235. https://doi.org/10.1016/j.epsl.2019.01.052.

Contreras, L., Pross, J., Bijl, P.K., O'Hara, R.B., Raine, J.I., Sluijs, A., Brinkhuis, H., 2014. Southern high-latitude terrestrial climate change during the Palaeocene-Eocene derived from a marine pollen record (ODP Site 1172, East Tasman Plateau). Clim. Past 10, 1401–1420. https://doi.org/10.5194/cp-10-1401-2014.

Cooper, W., Cooper, W., 2004. Fruits of the Australian tropical rainforest, Nokomis Publications, [Clifton Hill], Victoria.

Cramwinckel, M.J., Huber, M., Kocken, I.J., Agnini, C., Bijl, P.K., Bohaty, S.M., Frieling, J., Goldner, A., Hilgen, F.J., Kip, E.L., Peterse, F., van der Ploeg, R., Röhl, U., Schouten, S., Sluijs, A., 2018. Synchronous tropical and polar temperature evolution in the Eocene. Nature 559, 382–386. https://doi.org/10.1038/s41586-018-0272-2.

Deconto, R.M., Pollard, D., 2003. Rapid Cenozoic glaciation of Antarctica induced by declining atmospheric CO2. Nature 1317, 245–249. https://doi.org/10.1038/nature01290.

Elsworth, G., Galbraith, E., Halverson, G., Yang, S., 2017. Enhanced weathering and CO2 drawdown caused by latest Eocene strengthening of the Atlantic meridional overturning circulation. Nat. Geosci. 10, 213–216. https://doi.org/10.1038/ngeo2888.

Emanuel, W.R., Shugart, H.H., Stevenson, M.P., 1985. Climatic change and the broad-scale distribution of terrestrial ecosystem complexes. Clim. Chang. 7, 29–43. https://doi.org/10.1007/BF00139439.

Exon, N.F., Kennett, J.P., Malone, M.J., 2001. Proceedings of the Ocean Drilling Program, 189 initial reports. Ocean Drilling Program. https://doi.org/10.2973/odp.proc.ir.189.2001.

Exon, N.F., Kennett, J.P., Malone, M.J., 2004. Leg 189 Synthesis: Cretaceous–Holocene history of the Tasmanian Gateway. In: Exon, N.F., Kennett, J.P., Malone, M.J. (Eds.), Proceedings of the Ocean Drilling Program, 189 Scientific Results. https://doi.org/10.2973/odp.proc.sr.189.101.2004. Ocean Drilling Program.

Fick, S.E., Hijmans, R.J., 2017. WorldClim 2: new 1-km spatial resolution climate surfaces for global land areas. Int. J. Climatol. 37, 4302–4315. https://doi.org/10.1002/joc.5086.

Gaina, C., Müller, D.R., Royer, J.Y., Stock, J., Hardebeck, J., Symonds, P., 1998. The tectonic history of the Tasman Sea: a puzzle with 13 pieces. J. Geophys. Res. Solid Earth 103, 12413–12433. https://doi.org/10.1029/98jb00386.

Galeotti, S., DeConto, R., Naish, T., Stocchi, P., Florindo, F., Pagani, M., Barrett, P., Bohaty, S.M., Lanci, L., Pollard, D., Sandroni, S., Talarico, F.M., Zachos, J.C., 2016. Antarctic Ice Sheet variability across the Eocene-Oligocene boundary climate transition. Science (80-.) 352, 76–80. https://doi.org/10.1126/science.aab0669.

Ordination. In: Gauch, H.G. (Ed.), 1982. Multivariate Analysis in Community Ecology. Cambridge University Press, Cambridge, pp. 109–172. https://doi.org/10.1017/CBO9780511623332.

GBIF, 2022. GBIF Occurrence Download [Data Set] [WWW Document]. Glob. Biodivers. Inf. Facil. https://doi.org/10.15468/dl.avu5sk.

Goodall, D.W., 1954. Objective methods for the classification of vegetation. III. An essay in the use of factor analysis. Aust. J. Bot. 2, 304–324.

Gradstein, F.M., Ogg, J.G., Schmitz, M.D., Ogg, G.M., 2012. The Geologic Time Scale 2012. Geol. Time Scale 2, 437–1144.

Griener, K.W., Warny, S., 2015. Nothofagus pollen grain size as a proxy for long-term climate change: an applied study on Eocene, Oligocene, and Miocene sediments from Antarctica. Rev. Palaeobot. Palynol. 221, 138–143. https://doi.org/10.1016/j.revpalbo.2015.06.003.

Grimm, E.C., 1987. CONISS: a FORTRAN 77 program for stratigraphically constrained cluster analysis by the method of incremental sum of squares. Comput. Geosci. 13, 13–35. https://doi.org/10.1016/0098-3004(87)90022-7.

Grimm, E.C., 1990. Tilia and Tiliagraph. PC spreadsheet and graphics software for pollen data. INQUA Work. Gr. Data Handl. Methods, Newsl. 4, 5–7.

Hammer, Ø., Harper, D.A.T., Ryan, P.D., 2001. Past: Paleontological statistics software package for education and data analysis. Palaeontol. Electron. 4, 178.

Harbert, R.S., Nixon, K.C., 2015. Climate reconstruction analysis using coexistence likelihood estimation (CRACLE): a method for the estimation of climate using vegetation. Am. J. Bot. 102, 1277–1289. https://doi.org/10.3732/ajb.1400500.

Hartman, J.D., Sangiorgi, F., Salabarnada, A., Peterse, F., Houben, A.J.P., Schouten, S., Brinkhuis, H., Escutia, C., Bijl, P.K., 2018. Paleoceanography and ice sheet variability offshore Wilkes Land, Antarctica – Part 3: Insights from Oligocene-Miocene TEX86-based sea surface temperature reconstructions. Clim. Past 14, 1275–1297. https://doi.org/10.5194/cp-14-1275-2018.

Hayek, L.C., Buzas, M.A., 2010. Surveying Natural Populations. Columbia University Press, New York.

Hijmans, R.J., Phillips, S., Leathwick, J., Elith, J., 2017. dismo: Species distribution modelling. R Packag. version 1, 1.

Hill, R.S., 2017. History of the Australian Vegetation: Cretaceous to Recent. University of Adelaide Press. https://doi.org/10.20851/australian-vegetation.

Hill, P.J., Exon, N.F., 2004. Tectonics and basin development of the offshore Tasmanian area; incorporating results from deep ocean drilling. In: Exon, N.F., Kennett, J.P., Malone, M. (Eds.), The Cenozoic Southern Ocean; Tectonics, Sedimentation and Climate between Australia and Antarctica. Geophysical Monograph Series, 151. American Geophysical Union, Washington, p. 19.

Hill, R.S., Scriven, L.J., 1995. The angiosperm-dominated woody vegetation of Antarctica: a review. Rev. Palaeobot. Palynol. 86, 175–198. https://doi.org/10.1016/0034-6667(94)00149-E.

Hoem, F.S., Sauermilch, I., Hou, S., Brinkhuis, H., Sangiorgi, F., Bijl, P.K., 2021. Late Eocene–early Miocene evolution of the southern Australian subtropical front: a marine palynological approach. J. Micropalaeontol. 40, 175–193. https://doi.org/10.5194/jm-40-175-2021.

Hoem, F.S., Sauermilch, I., Aleksinski, A.K., Huber, M., Peterse, F., Sangiorgi, F., Bijl, P. K., 2022. Strength and variability of the Oligocene Southern Ocean surface temperature gradient. Commun. Earth Environ. 3, 322. https://doi.org/10.1038/s43247-022-00666-5.

Holdgate, G.R., Sluiter, I.R.K., Taglieri, J., 2017. Eocene-Oligocene coals of the Gippsland and Australo-Antarctic basins – Paleoclimatic and paleogeographic context and implications for the earliest Cenozoic glaciations. Palaeogeogr. Palaeoclimatol. Palaeoecol. https://doi.org/10.1016/j.palaeo.2017.01.035.

Hope, G.S., 1996. History of Nothofagus in New Guinea and New Caledonia. In: Veblen, T.T., Hill, R.S., Read, J. (Eds.), The Ecology and Biogeography of Nothofagus Forests. Yale University Press, New Haven and London, pp. 257–270.

Houben, A.J.P., Bijl, P.K., Sluijs, A., Schouten, S., Brinkhuis, H., 2019. Late Eocene Southern Ocean cooling and invigoration of circulation preconditioned Antarctica for full-scale glaciation. Geochem. Geophys. Geosyst. 20, 2214–2234. https://doi.org/10.1029/2019GC008182.

Hutchinson, D.K., Coxall, H.K., Lunt, D.J., Steinthorsdottir, M., De Boer, A.M., Baatsen, M., Von Der Heydt, A., Huber, M., Kennedy-Asser, A.T., Kunzmann, L., Ladant, J.B., Lear, C.H., Moraweck, K., Pearson, P.N., Piga, E., Pound, M.J., Salzmann, U., Scher, H.D., Sijp, W.P., Åliwińska, K.K., Wilson, P.A., Zhang, Z., 2021. The Eocene-Oligocene transition: a review of marine and terrestrial proxy data, models and model-data comparisons. Clim. Past. https://doi.org/10.5194/cp-17-269-2021.

Huurdeman, E.P., Frieling, J., Reichgelt, T., Bijl, P.K., Bohaty, S.M., Holdgate, G.R., Gallagher, S.J., Peterse, F., Greenwood, D.R., Pross, J., 2021. Rapid expansion of meso-megathermal rain forests into the southern high latitudes at the onset of the Paleocene-Eocene thermal Maximum. Geology 49, 40–44. https://doi.org/10.1130/G47343.1.

Katz, M.E., Miller, K.G., Wright, J.D., Wade, B.S., Browning, J.V., Cramer, B.S., Rosenthal, Y., 2008. Stepwise transition from the Eocene greenhouse to the Oligocene icehouse. Nat. Geosci. 1, 329–334. https://doi.org/10.1038/ngeo179.
Kennett, J.P., 1977. Cenozoic evolution of Antarctic glaciation, the circum-Antarctic Ocean, and their impact on global paleoceanography. J. Geophys. Res. 82, 3843–3860. https://doi.org/10.1029/jc082i027p03843.
Kershaw, A.P., 1988. Australasia. In: Huntley, B., Webb 111, T. (Eds.), Vegetation History. Kluwer Academic Publishers, Dordrecht, pp. 237–306.
Kershaw, P., Wagstaff, B., 2001. The southern conifer family Araucariaceae: history, status, and value for paleoenvironmental reconstruction. Annu. Rev. Ecol. Syst. 32, 397–414. https://doi.org/10.1146/annurev.ecolsys.32.081501.114059.
Klages, J.P., Salzmann, U., Bickert, T., Hillenbrand, C.D., Gohl, K., Kuhn, G., Bohaty, S. M., Titschack, J., Müller, J., Frederichs, T., Bauersachs, T., Ehrmann, W., van de Flierdt, T., Pereira, P.S., Larter, R.D., Lohmann, G., Niezgodzki, I., Uenzelmann-Neben, G., Zundel, M., Spiegel, C., Mark, C., Chew, D., Francis, J.E., Nehrke, G., Schwarz, F., Smith, J.A., Freudenthal, T., Esper, O., Pälike, H., Ronge, T.A., Dziadek, R., Afanasyeva, V., Arndt, J.E., Ebermann, B., Gebhardt, C., Hochmuth, K., Küssner, K., Najman, Y., Riefstahl, F., Scheinert, M., 2020. Temperate rainforests near the South Pole during peak Cretaceous warmth. Nature 580, 81–86. https://doi.org/10.1038/s41586-020-2148-5.
Korasidis, V.A., Wallace, M.W., Wagstaff, B.E., Hill, R.S., 2019. Terrestrial cooling record through the Eocene-Oligocene transition of Australia. Glob. Planet. Chang. 173, 61–72. https://doi.org/10.1016/j.gloplacha.2018.12.007.
Kühl, N., Gebhardt, C., Litt, T., Hense, A., 2002. Probability density functions as botanical-climatological transfer functions for climate reconstruction. Quat. Res. 58, 381–392. https://doi.org/10.1006/qres.2002.2380.
Larcher, W., Winter, A., 1981. Frost susceptibility of palms: experimental data and their interpretation. Principes 25, 143–155.
Lauretano, V., Kennedy-Asser, A.T., Korasidis, V.A., Wallace, M.W., Valdes, P.J., Lunt, D. J., Pancost, R.D., Naafs, B.D.A., 2021. Eocene to Oligocene terrestrial Southern Hemisphere cooling caused by declining pCO 2. Nat. Geosci. https://doi.org/10.1038/s41561-021-00788-z.
Lee, D.E., Lee, W.G., Jordan, G.J., Barreda, V.D., 2016. The Cenozoic history of New Zealand temperate rainforests: comparisons with southern Australia and South America. New Zeal. J. Bot. 54, 100–127. https://doi.org/10.1080/0028825X.2016.1144623.
Legendre, P., Legendre, F., 2012. Numerical Ecology, 3rd ed. Elsevier.
Liu, Z., Pagani, M., Zinniker, D., DeConto, R., Huber, M., Brinkhuis, H., Shah, S.R., Leckie, R.M., Pearson, A., 2009. Global cooling during the Eocene-Oligocene climate transition. Science (80-.) 323, 1187–1190. https://doi.org/10.1126/science.1166368.
Macphail, M.K., 2007. Australian Palaeoclimates: Cretaceous to Tertiary - A review of palaeobotanical and related evidence to the year 2000. CRC LEME Spec. Vol. Open File Rep. 151, 266pp.
Macphail, M., Cantrill, D.J., 2006. Age and implications of the Forest Bed, Falkland Islands, Southwest Atlantic Ocean: evidence from fossil pollen and spores. Palaeogeogr. Palaeoclimatol. Palaeoecol. 240, 602–629. https://doi.org/10.1016/j.palaeo.2006.03.010.
Macphail, M.K., Hill, R.S., 2018. What was the vegetation in northwest Australia during the Paleogene, 66–23 million years ago? Aust. J. Bot. 66, 556–574. https://doi.org/10.1071/BT18143.
Macphail, M., Alley, F., Truswell, E., Sluiter, I.R.K., 1994. Early Tertiary vegetation: evidence from spores and pollen. In: Hill, R.S. (Ed.), History of the Australian Vegetation: Cretaceous to Recent. Cambridge University Press, Cambridge, pp. 189–261.
Macphail, M.K., Pemberton, M., Jacobson, G., 1999. Peat mounds of southwest Tasmania: possible origins. Aust. J. Earth Sci. 46, 667–677. https://doi.org/10.1046/j.1440-0952.1999.00736.x.
Martin, H., 1994. Australian Tertiary phytogeography: evidence for palynology. In: Hill, R.S. (Ed.), History of the Australian Vegetation: Cretaceous to Holocene. Cambridge University Press, Cambridge, pp. 104–142.
Myerscough, P., Whelan, R., Bradstock, R., 2007. Ecology of Proteaceae with special reference to the Sydney region. Cunninghamia 6, 951–1015.
Naafs, B.D.A., Inglis, G.N., Zheng, Y., Amesbury, M.J., Biester, H., Bindler, R., Blewett, J., Burrows, M.A., del Castillo Torres, D., Chambers, F.M., Cohen, A.D., Evershed, R.P., Feakins, S.J., Gałka, M., Gallego-Sala, A., Gandois, L., Gray, D.M., Hatcher, P.G., Honorio Coronado, E.N., Hughes, P.D.M., Huguet, A., Könönen, M., Laggoun-Défarge, F., Lähteenoja, O., Lamentowicz, M., Marchant, R., McClymont, E., Pontevedra-Pombal, X., Ponton, C., Pourmand, A., Rizzuti, A.M., Rochefort, L., Schellekens, J., De Vleeschouwer, F., Pancost, R.D., 2017. Introducing global peat-specific temperature and pH calibrations based on brGDGT bacterial lipids. Geochim. Cosmochim. Acta 208, 285–301. https://doi.org/10.1016/j.gca.2017.01.038.
Oksanen, J., Blanchet, F.G., Friendly, M., Kindt, R., Legendre, P., McGlinn, D., Minchin, P.R., O'Hara, R.B., Simpson, G.L., Solymos, P., Stevens, M.H.H., Szoecs, E., Wagner, H., 2019. Vegan: community ecology package [WWW Document]. R Packag. version 2.5–6. URL. https://cran.r-project.org/package=vegan (accessed 8.9.21).
Pagani, M., Zachos, J.C., Freeman, K.H., Tipple, B., Bohaty, S., 2005. Marked decline in atmospheric carbon dioxide concentrations during the paleogene. Science (80-.) 309, 600–603. https://doi.org/10.1126/science.1110063.
Pälike, H., Norris, R.D., Herrle, J.O., Wilson, P.A., Coxall, H.K., Lear, C.H., Shackleton, N. J., Tripati, A.K., Wade, B.S., 2006. The heartbeat of the Oligocene climate system. Science (80-.) 314, 1894–1898. https://doi.org/10.1126/science.1133822.
Panitz, S., Salzmann, U., Risebrobakken, B., De Schepper, S., Pound, M.J., 2016. Climate variability and long-term expansion of peatlands in Arctic Norway during the late Pliocene (ODP Site 642, Norwegian Sea). Clim. Past 11 (6), 5755–5798.
Partridge, A., Dettmann, M., 2003. Plant microfossils. In: Birch, W.D. (Ed.), Geology of Victoria. Geological Society of Australia Special Publication, pp. 639–652.
Pearson, P.N., Foster, G.L., Wade, B.S., 2009. Atmospheric carbon dioxide through the Eocene–Oligocene climate transition. Nature 461, 1110–1113. https://doi.org/10.1038/nature08447.
Pfuhl, H.A., McCave, I.N., 2003. Integrated Age Models for the Early Oligocene–Early Miocene, Sites 1168 and 1170-1172. Proc. Ocean Drill. Program, 189 Sci. Results 1–21. https://doi.org/10.2973/odp.proc.sr.189.108.2003.
Pocknall, D.T., 1989. Late Eocene to early Miocene vegetation and climate history of New Zealand. J. R. Soc. New Zeal. 19, 1–18. https://doi.org/10.1080/03036758.1989.10426451.
Prebble, J.G., Raine, J.I., Barrett, P.J., Hannah, M.J., 2006. Vegetation and climate from two Oligocene glacioeustatic sedimentary cycles (31 and 24 Ma) cored by the Cape Roberts Project, Victoria Land Basin, Antarctica. Palaeogeogr. Palaeoclimatol. Palaeoecol. 231, 41–57. https://doi.org/10.1016/j.palaeo.2005.07.025.
Pound, M.J., Salzmann, U., 2017. Heterogeneity in global vegetation and terrestrial climate change during the late Eocene to early Oligocene transition. Sci. Rep. 7, 43386. https://doi.org/10.1038/srep43386.
Prebble, J.G., Kennedy, E.M., Reichgelt, T., Clowes, C., Womack, T., Mildenhall, D.C., Raine, J.I., Crouch, E.M., 2021. A 100 million year composite pollen record from New Zealand shows maximum angiosperm abundance delayed until Eocene. Palaeogeogr. Palaeoclimatol. Palaeoecol. 566 https://doi.org/10.1016/j.palaeo.2020.110207.
Prider, J.N., Christophel, D.C., 2000. Distributional ecology of Gymnostoma australianum (Casuarinaceae), a putative palaeoendemic of Australian wet tropic forests. Aust. J. Bot. 48, 427–434. https://doi.org/10.1071/BT99006.
Pross, J., Contreras, L., Bijl, P.K., Greenwood, D.R., Bohaty, S.M., Schouten, S., Bendle, J. A., Röhl, U., Tauxe, L., Raine, J.I., Huck, C.E., Van De Flierdt, T., Jamieson, S.S.R., Stickley, C.E., Van De Schootbrugge, B., Escutia, C., Brinkhuis, H., Escutia Dotti, C., Klaus, A., Fehr, A., Williams, T., Bendle, J.A.P., Carr, S.A., Dunbar, R.B., Gonzèlez, J. J., Hayden, T.G., Iwai, M., Jimenez Espejo, F.J., Katsuki, K., Soo Kong, G., Mc Kay, R. M., Nakai, M., Olney, M.P., Passchier, S., Pekar, S.F., Riesselman, C.R., Sakai, T., Shrivastava, P.K., Sugisaki, S., Tuo, S., Welsh, K., Yamane, M., 2012. Persistent near–tropical warmth on the antarctic continent during the early eocene epoch. Nature 488, 73–77. https://doi.org/10.1038/nature11300.
Quilty, P.G., 2001. Late Eocene foraminifers and palaeoenvironment, Cascade Seamount, southwest Pacific Ocean: Implications for seamount subsidence and Australia Antarctica Eocene correlation. Aust. J. Earth Sci. 48, 633–641. https://doi.org/10.1046/j.1440-0952.2001.485886.x.
R Core Team, 2019. R: A Language and Environment for Statistical Computing [WWW Document]. R Found. Stat. Comput. URL. https://www.r-project.org/ (accessed 8.9.21).
Raine, J.I., Askin, R.A., 2001. Terrestrial palynology of Cape Roberts Project drillhole CRP-3, Victoria Land Basin, Antarctica. Terra Antart. 8, 389–400.
Raine, J.C., Mildenhall, D.C., Kennedy, E.M., 2011. New Zealand fossil spores and pollen: an illustrated catalogue. GNS Sci. Misc. Ser. 4, 1–25.
Read, J., Hope, G.S., Hill, R.S., 2005. Phytogeography and climate analysis of Nothofagus subgenus Brassospora in New Guinea and New Caledonia. Aust. J. Bot. 53, 297–312. https://doi.org/10.1071/BT04155.
Reichgelt, T., West, C.K., Greenwood, D.R., 2018. The relation between global palm distribution and climate. Sci. Rep. 2–12 https://doi.org/10.1038/s41598-018-23147-2.
Sanguinetti, J., Kitzberger, T., 2008. Patterns and mechanisms of masting in the large-seeded southern hemisphere conifer Araucaria araucana. Austral Ecol. 33, 78–87. https://doi.org/10.1111/j.1442-9993.2007.01792.x.
Sauermilch, I., Whittaker, J.M., Bijl, P.K., Totterdell, J.M., Jokat, W., 2019. Tectonic, oceanographic, and climatic controls on the cretaceous-cenozoic sedimentary record of the Australian-Antarctic Basin. J. Geophys. Res. Solid Earth 124, 7699–7724. https://doi.org/10.1029/2018JB016683.
Sauermilch, I., Whittaker, J.M., Klocker, A., Munday, D.R., Hochmuth, K., Bijl, P.K., LaCasce, J.H., 2021. Gateway-driven weakening of ocean gyres leads to Southern Ocean cooling. Nat. Commun. 12, 6465. https://doi.org/10.1038/s41467-021-26658-1.
Seppelt, R.D., 2006. Sphagnaceae. In: Flora of Australia Volume 51 (Mosses 1). ABRS & CSIRO Publishing, Canberra & Melbourne, pp. 89–104.
Shannon, C.E., 1948. A mathematical theory of communication. Bell Syst. Tech. J. 27, 379–423. https://doi.org/10.1002/j.1538-7305.1948.tb01338.x.
Shipboard Scientific Party, 2001. Leg 189 Summary. In: Proceedings of the Ocean Drilling Program, 189 Initial Reports. Ocean Drilling Program.. https://doi.org/10.2973/odp.proc.ir.189.101.2001.
Sijp, W.P., England, M.H., Huber, M., 2011. Effect of the deepening of the Tasman Gateway on the global ocean. Paleoceanography 26, 1–18. https://doi.org/10.1029/2011PA002143.
Sijp, W.P., von der Heydt, A.S., Dijkstra, H.A., Flögel, S., Douglas, P.M.J., Bijl, P.K., 2014. The role of ocean gateways on cooling climate on long time scales. Glob. Planet. Chang. https://doi.org/10.1016/j.gloplacha.2014.04.004.
Sluijs, A., Brinkhuis, H., Stickley, C.E., Warnaar, J., Williams, G.L., Fuller, M., 2003. Dinoflagellate cysts from the Eocene–Oligocene transition in the Southern Ocean: results from ODP Leg 189. In: Proceedings of the Ocean Drilling Program, 189 Scientific Results. Ocean Drilling Program, pp. 1–42. https://doi.org/10.2973/odp.proc.sr.189.104.2003.
Sluiter, I.R.K., Holdgate, G.R., Reichgelt, T., Greenwood, D.R., Kershaw, A.P., Schultz, N. L., 2022. A new perspective on Late Eocene and Oligocene vegetation and

paleoclimates of South-eastern Australia. Palaeogeogr. Palaeoclimatol. Palaeoecol. 596, 110985 https://doi.org/10.1016/j.palaeo.2022.110985.
Steane, D.A., Wilson, K.L., Hill, R.S., 2003. Using matK sequence data to unravel the phylogeny of Casuarinaceae. Mol. Phylogenet. Evol. 28, 47–59. https://doi.org/10.1016/S1055-7903(03)00028-9.
Stickley, C.E., Brinkhuis, H., Schellenberg, S.A., Sluijs, A., Röhl, U., Fuller, M., Grauert, M., Huber, M., Warnaar, J., Williams, G.L., 2004. Timing and nature of the deepening of the Tasmanian Gateway. Paleoceanography 19, 1–18. https://doi.org/10.1029/2004PA001022.
ter Braak, C.J.F., Šmilauer, P., 2002. CANOCO Reference Manual and CanoDraw for Windows User's Guide: Software for Canonical Community Ordination.
Thompson, N., Salzmann, U., López-Quirós, A., Bijl, P.K., Hoem, F.S., Etourneau, J., Sicre, M.-A., Roignant, S., Hocking, E., Amoo, M., Escutia, C., 2022. Vegetation change across the Drake Passage region linked to late Eocene cooling and glacial disturbance after the Eocene–Oligocene transition. Clim. Past 18, 209–232. https://doi.org/10.5194/cp-18-209-2022.
Tibbett, E.J., Scher, H.D., Warny, S., Tierney, J.E., Passchier, S., Feakins, S.J., 2021. Late Eocene record of hydrology and temperature from Prydz Bay, East Antarctica. Paleoceanogr. Paleoclimatol. 36 https://doi.org/10.1029/2020PA004204.
Tomlinson, P.B., 2006. The uniqueness of palms. Bot. J. Linn. Soc. 151, 5–14. https://doi.org/10.1111/j.1095-8339.2006.00520.x.
van Hinsbergen, D.J.J., de Groot, L.V., van Schaik, S.J., Spakman, W., Bijl, P.K., Sluijs, A., Langereis, C.G., Brinkhuis, H., 2015. A Paleolatitude Calculator for Paleoclimate Studies. PLoS One 10, 1–21. https://doi.org/10.1371/journal.pone.0126946.
Villa, G., Fioroni, C., Persico, D., Roberts, A.P., Florindo, F., 2014. Middle Eocene to Late Oligocene Antarctic glaciation/deglaciation and Southern Ocean productivity. Paleoceanography 29, 223–237. https://doi.org/10.1002/2013PA002518.
Westerhold, T., Marwan, N., Drury, A.J., Liebrand, D., Agnini, C., Anagnostou, E., Barnet, J.S.K., Bohaty, S.M., De Vleeschouwer, D., 2020. An Astronomically Dated Record of Earth ' S Climate and its Predictability over the Last 66 Million Years 1387, 1383–1387.
Willard, D.A., Donders, T.H., Reichgelt, T., Greenwood, D.R., Sangiorgi, F., Peterse, F., Nierop, K.G.J., Frieling, J., Schouten, S., Sluijs, A., 2019. Arctic vegetation, temperature, and hydrology during Early Eocene transient global warming events. Glob. Planet. Chang. 178, 139–152. https://doi.org/10.1016/j.gloplacha.2019.04.012.
Zachos, J., Pagani, H., Sloan, L., Thomas, E., Billups, K., 2001. Trends, rhythms, and aberrations in global climate 65 Ma to present. Science (80-.). https://doi.org/10.1126/science.1059412.
Zhang, Y.G., Henderiks, J., Liu, X., 2020. Refining the alkenone-pCO2 method II: Towards resolving the physiological parameter 'b'. Geochim. Cosmochim. Acta 281, 118–134. https://doi.org/10.1016/j.gca.2020.05.002.